Mechanics of Bistable Two-Shelled Composite Booms

Andrew J. Lee[*]
University of Michigan, Ann Arbor, MI 48109, USA

and

Juan M. Fernandez[†]
NASA Langley Research Center, Hampton, VA 23681, USA

The phenomenon of bistability in single-walled composite cylindrical shells or slit tubes has been extensively studied with detailed models that represent the mechanics of these structures as they undergo large deformations from the extended to the stored state and vice versa. This study focuses on the mechanics of bistable composite booms that are formed by coupling or bonding two thin shells. A two-parameter inextensional analytical model is used to describe the behavior of the various two-shelled structures and find laminates and shell geometries of interest that induce bistability. The natural coiled diameters of all boom types are predicted analytically and compared with preliminary experimental data. Using the derived model, parametric analysis is conducted to determine optimal boom geometries that maximize stiffnesses and meet system requirements while retaining bistability.

I.   Introduction

Slit-tube booms have been a popular type of deployable structure for space applications since they were first used in 1961 on-board the Canadian Alouette I spacecraft as dipole antennas[1]. Since then, the Storable Tubular Extendible Member (STEM) family of booms have been used on many occasions as antennas, gravity gradient booms, grasping devices, docking booms, and to manipulate external payloads. Tape-springs, slit tubes and STEMs are thin cylindrical shell structures that differ on their subtended angle, α. While tape-springs subtend smaller angles of about $\alpha < 225°$, slit tubes have $225° \leq \alpha \leq 360°$, and STEMs can have some degree of overlap so that $\alpha > 360°$. These deployables can be flattened and coiled for storage, resulting in high deployed-to-stored length ratios ideal for applications with stringent volume requirements. These structures are monostable as they are only stable in their as-manufactured extended state. A secondary stable coiled state can be induced in isotropic shells through the introduction of an initial 'prestress' in the structure[2], and in composite cylindrical shells by careful selection of the lay-up and fiber orientations[3]. Bistability in thin shells is an example of bio-mimicry, inspired by the closure-opening mechanism of the Venus Flytrap leaf[5]. This enables useful compact deployment mechanism designs that reduce overall system mass and volume[4]; critical for small satellite applications. In the late 1990's, RolaTube Technology Ltd. commercialized bistable composite tape-springs and slit tubes under the trademark name "Bistable Reeled Composites" (BRC)[6].

In order to achieve bistability in composite cylindrical shells, stiff fibers are placed at such an angle to the longitudinal axis that the shell exhibits anisotropic bending properties. The second stable state will then favor equal-sense bending[7], meaning that the center of curvature of the shell in both stable states is on the same side of the surface. Each of the two stable states is a strain energy minimum, with the extended configuration existing in the lower of the two energy states. Bistable shell structures undergo a transition between the two strain energy minima requiring the input of work. Once a certain transition point has been passed, the structure will follow the negative strain energy gradient to the other stable state. The energy gradient between the two stable states is tailored by the laminate and geometry of the shell to tune the release of energy for the requirements of a certain application.

Several different concepts of deployable composite tape-springs and slit tubes with differing energy gradients between the stable states have been proposed. For example, in semi-neutrally stable shells, both the extended and

---

[*] PhD Candidate, Department of Aerospace Engineering, University of Michigan, 1320 Beal Ave., Ann Arbor, MI 48109. AIAA Student Member.
[†] Research Aerospace Engineer, Structural Dynamics Branch, NASA LaRC, 4 West Taylor Street, Mail Stop 230. AIAA Member.

coiled configuration are zero energy points, meaning that a partially unrolled tube will neither extend or coil up[8]. Neutrally stable tubes have a zero energy gradient between the deployed and stowed states, resulting in a resilient structure that is easy to control, can be fully or partially re-stowed, avoiding deployment shocks[9]. It is also possible to construct a bistable composite shell with the coiled/stowed state representing the lower of the two energy minima, favoring retractability. As the length of the tube increases, the diameter of the coil expands to a point where bistability is lost. In order to retain bistability, a new design approach was developed[10]. These boom structures that are now bistable over the whole length (BOWL) have each section of the long boom in a different strain energy state. This results in the length-wise anisotropy of the shell laminate tailored to produce a bistable spiral-shaped coil, which accounts for the thickness of the shell, rather than a bistable cylindrical-shaped coil with a fixed diameter[3,11-13].

Previous work has mainly focused on introducing bistability in single-thin-walled structures such as tape springs, slit tubes, and STEMs. The study presented in this paper investigates how bistable configurations were achieved in thin two-shelled composite structures; booms that have a cross-section formed by coupling, joining or bonding two thin composite shells.
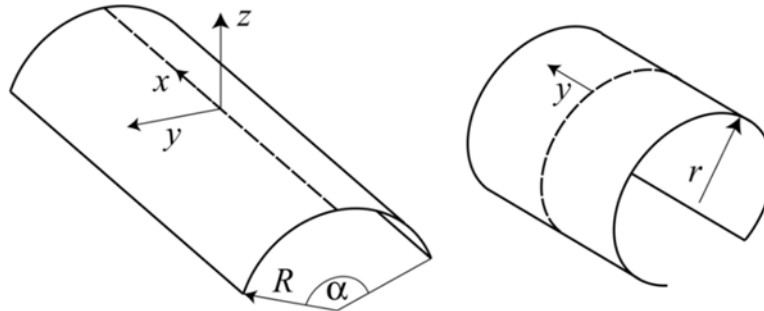
Fig. 1. A section of thin-shell bistable tape-spring in the initial, extended, stable configuration (left), and the second, coiled, stable state (right). *x, y* and z are the longitudinal, transverse and out-of-plane directions of the extended shell. *R* and *r* are the extended and coiled radius of curvature, respectively, and *α* is the subtended angle of the cross-section.

II.   Bistable Two-shelled Composite Booms

Several deployable composite boom concepts are currently being developed for 5-20 m long structural systems for small satellites[14]. These booms only have a single stable state, the as-manufactured monostable configuration. In order to develop booms that require less mechanical packaging management during the coiled configuration with reliable self-deployable architectures having predictable deployment dynamics, an effort to introduce bistability in these types of two-shelled structures was initated.

A. Bi-SHEARLESS Boom

The SHEAth-based Rollable LEnticular-Shaped and low-Friction (SHEARLESS) composite boom consists of two independent composite opposed tape-springs forming a biconvex shape inside a low-friction polymer sheath, which acts as an effective coupling sleeve[14-17]. Relative motion or sliding of the thin-shell tape-springs during coiling/deployment inside the sheath is required, Fig. 2 (a), enabling a more compact package when compared to other two-shelled bonded booms of equivalent overall thickness. Upon deployment, the edges of the tape-springs couple, Fig. 2 (b), forming a semi-closed double-symmetrical cross-section with improved torsional and bending stiffness. Bistable configurations of this type of boom, named Bi-SHEARLESS, have been produced by engineering the shell laminates[15]. For this, both shells have to coil opposite of each other with the outer shell being bistable (equal-sense coiled) and the inner shell (opposite-sense coiled) being flexible and compliant enough to prevent the outer bistable shell snaping-through while in the coiled state. The secondary stable coiled diameter for a given boom geometry and bistable laminate of the outer shell can be tailored by the bending stiffness, D_{11i}, of the inner shell.

Fig. 2 (c) exemplifies how the secondary stable diameter of the coil grows when an external sheath couples a bistable tape-spring (28 mm natural coiled diameter) as the outer shell with a monostable tape-spring as the inner shell to form a Bi-SHEARLESS boom (65 mm natural coiled diameter). Another way to tailor the secondary stable diameter of the coil for a fixed outer-to-inner-shell bending stiffness ratio (D_{11o}/D_{11i}) is by changing the boom cross-section design to increase/decrease the principal moments of area (I_{yy} and I_{zz}). Fig. 2 (d) shows a coiled Bi-SHEARLESS boom that has a shallow cross-section of *R =25 mm* and *α = 101°*. Such boom has a stable coiled diameter of 75 mm,

American Institute of Aeronautics and Astronautics

much larger than the 38 mm diameter that a deeper cross-section design (of the same laminate construction) with $R = 16\ mm$ and $\alpha = 161°$ would result in. Note that there will also be a boom design limit for which shallower cross-sections will cease to yield bistable biconvex booms.

(a)   (b)   (c)   (d)
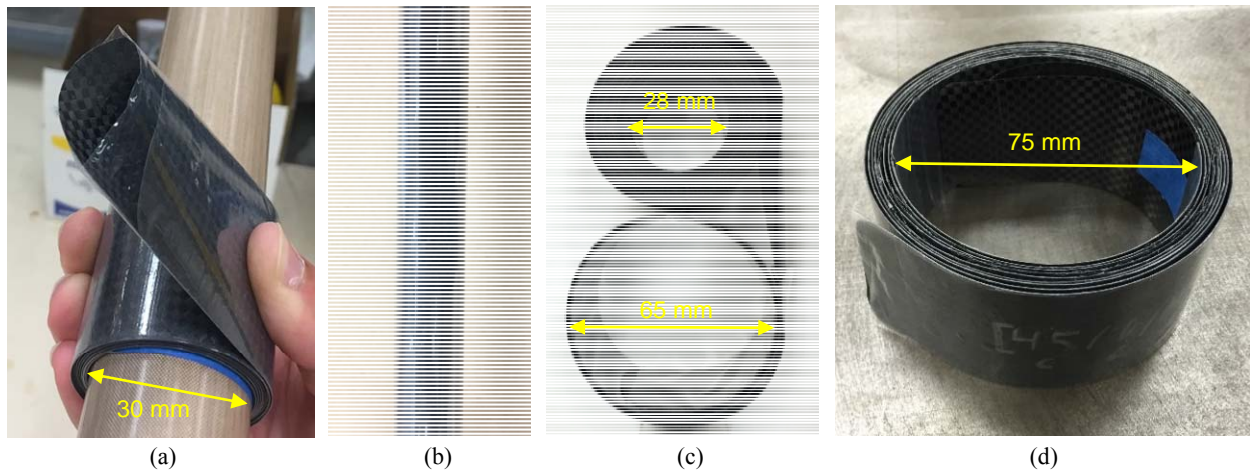
Fig. 2. (a) SHEARLESS boom wrapped, showing the relative offset between tape-springs; (b) coupled edges of the tape-springs in the deployed configuration; (c) bistable tape-spring wrapped (top) used as the outer shell of a Bi-SHEARLESS boom (bottom), showing the size difference in stable coiled diameter; (d) coiled Bi-SHEARLESS boom with a shallow cross-section design ($\alpha = 101°$).

B. Bi-TRAC Boom

The Triangular Rollable And Collapsible (TRAC) boom has an architecture with a large cross-section moment of area to packaged height ratio, making them ideal for small satellite applications[18]. The triangular cross-section shape is presented in Fig. 3 (a), and a single bonded area (web) at one end of the boom results in two long flanges that increase the boom moment of area. Recent interest in this boom concept has resulted in ever-lighter TRAC boom designs using state-of-the-art thin-ply composite materials[14,19,20].

(a)   (b)   (c)
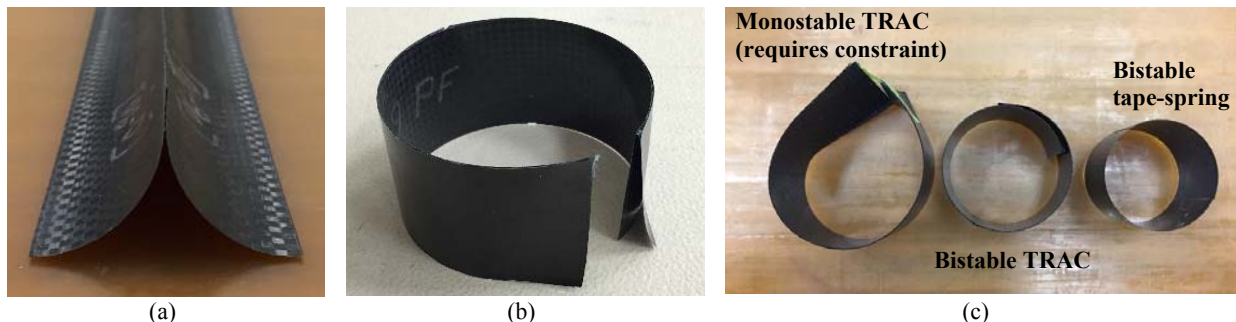
Fig. 3 (a) Cross-section shape of a deployed TRAC boom; (b) Bi-TRAC boom in a stable coiled state; (c) Comparison of bistable and monostable coiled booms. The Bi-TRAC coiled behavior is similar to that of standard bistable tape-spring and requires no constraints while rolled.

Bistability in this boom concept has been achieved[14] using the same design approach previously mentioned for the Bi-SHEARLESS booms, i.e. producing non-symmetrical boom constructions with respect to its X-Y plane of symmetry by having dissimilar shell laminates. In this case, the inner shell of the boom, that has to coil in an equal-sense way around the drum, is made with a bistable laminate, bounding the natural coiling diameter of the whole boom. The outer shell, that has to coil in a more energetic opposite-sense way, is made with a less stiff monostable laminate with a large strain-to-failure laminate. During boom packaging, the naturally bistable half side encloses the monostable half side at each overlap. By managing the strain energy of the outer flange, bifurcation to the extended state during boom deployment only occurs on the unrestricted outermost wrap of the coil. In addition, there is a strain energy minimum state in the coiled configuration acting against bifurcation of the inner flange that normally drives the maximum and minimum coiled diameters of TRAC booms along with fiber failure[19,20].

C. Bi-X Boom

The X-Boom[21] shape takes after a TRAC geometry, but the bond (web) occurs at the center of the shells, rather than on one edge of the boom, forming four flanges with the cross-section resembling the letter "X". Although the area moment of inertia per unit of packaged height was reduced compared with the TRAC boom shape, the cross-section becomes double-symmetrical, and decouples bending and torsion deformations on a boom resulting in an open-section structure with low torsional stiffness. The monostable X-boom is being considered by Analytical Mechanics Associates, Inc. as the extendable boom structure for a new solar array concept[22].

Achieving bistable designs for the X-Boom geometry is more restrictively challenging than for TRAC booms of the same flattened height, given the shallower flanges and the higher tendency of both inner flanges to locally buckle upon coiling.

D. Bi-CTM Boom

The Collapsible Tubular Mast (CTM, also known as lenticular boom) is the most widely-used closed-section thin-shell rollable boom. Its mechanical performance makes it ideal for structural applications that require high dimensional stability. NASA is currently investing in developing high-performance thin-ply composite CTM booms that will be used for deployable structures on interplanetary small satellite missions[23,24].

The CTM boom geometry consists of joining two omega-shaped shells at two flat regions on each shell edge, called the web. The cross-section of each omega shell can be defined by three circular or parabolic arcs, plus the two straight sections. In the 45-mm-tall booms initially developed for NASA's Near Earth Asteroid (NEA) Scout solar sail mission[14,24], these omega shells were formed by three equal circular segments with a subtended angle $\alpha = 85°$, and taller versions for larger sail systems will have omega-shaped shells formed by dissimilar segments radii, as shown in Fig. 4.
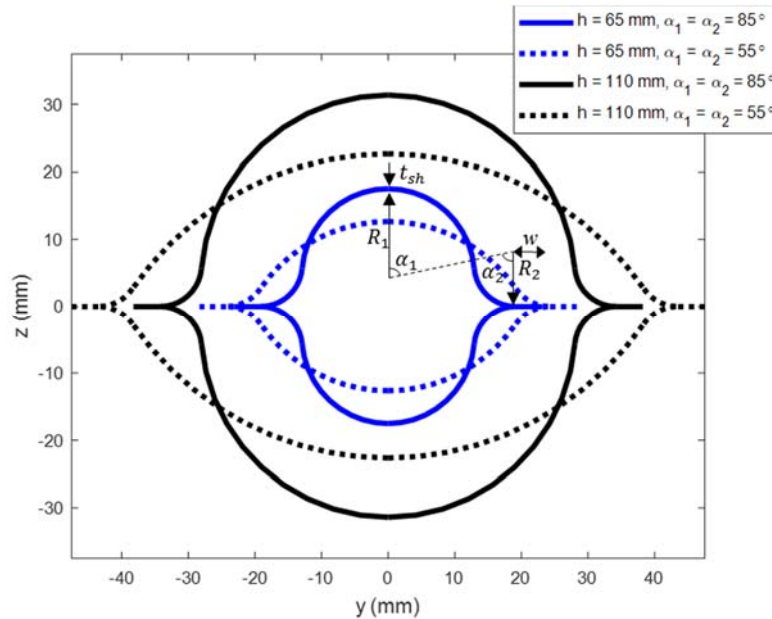
Fig. 4. Cross-section shapes of two CTM booms with a flattened height of *h = 65 mm* (blue lines) and *h = 110 mm* (black lines). For each boom size, two cross-sections of subtended angles *α = 85°* (solid lines) and *α = 55°* (dashed lines) are shown.

The current goal is to study if bistable designs of the CTM are indeed possible given the complex geometry of the structure. Cases where the boom geometric symmetry about the bonding line is maintained (same omega-shell geometry), as in Fig. 4, are being investigated with the shell composite laminate for each boom half being different in all cases. In general, the shell segments that need to be coiled in an equal-sense way, such as those corresponding to radius R_1 of the outer shell and radius R_2 of the inner shell, made from a bistable laminate. The shell segments that need to be coiled in an opposite-sense way, such as those corresponding to radius R_2 of the outer shell and radius R_1 of the inner shell, will be made from a more compliant laminate.

III. Inextensional Model

A simple analytical method of predicting the extended and coiled configurations of composite cylindrical shells[13] was adopted and extended here to predict the stable coiled diameter and strain energy state of two-shelled composite booms. It assumes that the initial configuration of the shell is stress free and otherwise the shell is under plane stress. In addition, the shell's mid-surface bends without stretch, which means that all deformations are uniform, inextensional, and the Gaussian curvature remains unchanged. This implies that every possible configuration of the shell can be fitted to the surface of a cylinder, as shown in Fig. 5. Thus, these configurations can be defined by only two parameters, which are the curvature C of the underlying cylinder and the orientation θ of the shell relative to the cylinder's axis.
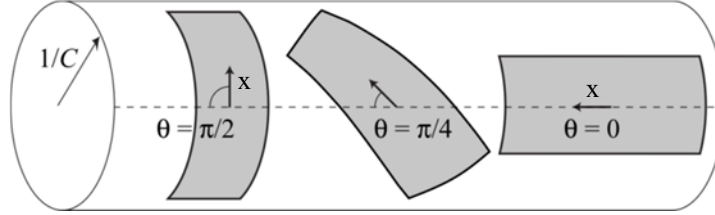
Fig. 5. Coordinate system defining shell configurations on an underlying cylinder of curvature C.

A. Bi-SHEARLESS Boom

For the case of two-shelled booms without any flat bonded areas and identical cylindrical shell radii, Bi-SHEARLESS booms, each shell's non-dimensionalized changes in curvature between the initially extended configuration at $\theta = 0$ and $1/C = R$, and the final configuration at $0 < \theta < \pi$ are defined in Eq. 1. The $_O$ and $_I$ subscripts denote the outer and inner shells, that deform in the equal-sense and opposite-sense ways, respectively. Thus, the direction of κ_x flips between these two shells where it is positive for the outer shell and negative for the inner shell.

$$\widehat{\boldsymbol{k}}_{O,I} = R\Delta \begin{bmatrix} \kappa_x \\ \kappa_y \\ \kappa_{xy} \end{bmatrix} = \frac{CR}{2} \begin{bmatrix} \pm(1 - \cos 2\theta) \\ \cos 2\theta + 1 - \frac{2}{CR} \\ 2\sin 2\theta \end{bmatrix} \tag{1}$$

The strain energy contributors from the Bi-SHEARLESS boom are its inner and outer composite shells alone, and the sleeve's contribution is assumed to be negligible. All non-dimensional variables are written with a hat and defined in Eq. 2. These are used in the boom bending strain energy per unit length as defined in Eq. 3, which is non-dimensionalized in terms of the total bending stiffness in the x-direction $D_{O_{11}} + D_{I_{11}}$, the initial radius of curvature R, and the flattened height of each shell, h.

$$\widehat{U} = \frac{UR^2}{h(D_{O_{11}} + D_{I_{11}})}, \quad \widehat{\boldsymbol{D}}_{O,I} = \frac{\boldsymbol{D}_{O,I}}{D_{O_{11}} + D_{I_{11}}}, \quad \hat{C} = CR \tag{2}$$

$$\widehat{U} = \frac{1}{2}\left(\widehat{\boldsymbol{k}}_O^T \widehat{\boldsymbol{D}}_O \widehat{\boldsymbol{k}}_O + \widehat{\boldsymbol{k}}_I^T \widehat{\boldsymbol{D}}_I \widehat{\boldsymbol{k}}_I\right) \tag{3}$$

It should be noted that the $\boldsymbol{D}$ matrix of each shell is the reduced bending stiffness matrix from Classical Lamination Theory (CLT) defined in Eq. 4, allowing coupling between bending and stretching in case any of the studied shells have a non-zero $\boldsymbol{B}$ matrix. If $\boldsymbol{B} = \boldsymbol{0}$, $\boldsymbol{D}^*$ reduces to $\boldsymbol{D}$ and the in-plane strains are zero.

$$\boldsymbol{D}^* = \boldsymbol{D} - \boldsymbol{B}^T \boldsymbol{A}^{-1} \boldsymbol{B} \tag{4}$$

B. Bi-TRAC and Bi-X Booms

The bending strain energy terms of the Bi-TRAC and Bi-X booms correspond to their web and flange sections, made up of both inner and outer shells of identical shell radii. The web is the flat bonded region between both shells while the flanges have the initial radius of curvature R. Following the actual manufacturing approach, it is assumed that R of the flange is identical to the radius of the entire shell prior to bonding. The non-dimensional changes in

American Institute of Aeronautics and Astronautics

curvature of the web sections is given below, while the flange's $\widehat{\boldsymbol{k}}_f$ is Eq. 1, but with the direction of κ_x flipped between the inner and outer shells as these shells bend in the opposite-sense and equal-sense ways for these booms.

$$\widehat{\boldsymbol{k}}_w = \frac{\hat{c}}{2}\begin{bmatrix} 1 - \cos 2\theta \\ 0 \\ 2\sin 2\theta \end{bmatrix} \tag{5}$$

The Bi-TRAC boom's bending strain energy per unit length defined in Eq. 7 is non-dimensionalized with the parameters in Eq. 6, where the web width is w and the subscript $_A$ denotes the adhesive layer. Assuming the top and bottom flanges of the Bi-X boom have the same cross sectional geometries (double-symmetrical boom), its bending strain energy per unit length is also defined by Eq. 7.

$$\widehat{U} = \frac{UR^2}{h\left(D_{O_{11}}+D_{I_{11}}+D_{A_{11}}\right)}, \quad \widehat{\boldsymbol{D}}_{O,I,A} = \frac{\boldsymbol{D}_{O,I,A}}{D_{O_{11}}+D_{I_{11}}+D_{A_{11}}}, \quad \hat{C} = CR \tag{6}$$

$$\widehat{U} = \frac{1}{2h}\left[(h-w)\left(\widehat{\boldsymbol{k}}_{f_O}^T\widehat{\boldsymbol{D}}_O\widehat{\boldsymbol{k}}_{f_O} + \widehat{\boldsymbol{k}}_{f_I}^T\widehat{\boldsymbol{D}}_I\widehat{\boldsymbol{k}}_{f_I}\right) + w\widehat{\boldsymbol{k}}_w^T\left(\widehat{\boldsymbol{D}}_O + \widehat{\boldsymbol{D}}_I + \widehat{\boldsymbol{D}}_A\right)\widehat{\boldsymbol{k}}_w\right] \tag{7}$$

C. Circular Bi-CTM Boom

For the Bi-CTM with circular segments, the parameters of its cross sectional geometry are established in order to determine the strain energy terms of each shell segment. For both the inner and outer shells, let segment 1 be associated with R_1 and α_1 and segment 2 with R_2 and α_2, as shown in Fig. 4. To maintain tangent continuity and prevent kinks between segments 1 and 2, α_1 must equal α_2, which means only a single subtended angle and either R_1 or R_2 can be specified. Using the circular arc length equations and the relationship between h, w, and the arc lengths of segments 1 and 2 as given by L_1 and L_2 shown below, the unspecified radius is found. Tangent continuity cannot be guaranteed if both radii are specified instead.

$$h = 2(w + L_1 + L_2) \tag{8}$$

$$L_{1,2} = R_{1,2}\alpha_{1,2} \tag{9}$$

To allow varying cross-sectional geometries for the Bi-CTM, the radii, lengths, subtended angles of each shell segment are differentiated between the outer and inner shells. Only the flattened height and web widths are identical between the two shells. Assuming the initial manufactured radius of each segment does not change after bonding, the non-dimensional changes in curvature of segments 1 and 2 for both the outer and inner shells are given below.

$$\widehat{\boldsymbol{k}}_{1_{O,I}} = \frac{\hat{C}R_{1_{O,I}}}{2R_{1_O}}\begin{bmatrix} \pm(1 - \cos 2\theta) \\ \cos 2\theta + 1 - \frac{2}{\hat{C}} \\ 2\sin 2\theta \end{bmatrix} \tag{10}$$

$$\widehat{\boldsymbol{k}}_{2_{O,I}} = \frac{\hat{C}R_{2_{O,I}}}{2R_{1_O}}\begin{bmatrix} \mp(1 - \cos 2\theta) \\ \cos 2\theta + 1 - \frac{2}{\hat{C}} \\ 2\sin 2\theta \end{bmatrix} \tag{11}$$

The changes in curvature of the web section is given by Eq. 5 and every shell segment is normalized by R_{1_O} with $\hat{C} = CR_{1_O}$. This assumes that the changes in curvature of each segment is linearly proportional to that of the outer shell segment 1 based on the ratio of radii between the segments. The equal-sense and opposite-sense bending directions of each shell segment is accounted for in the direction of the κ_x. By summing the strain energy terms of every shell segment and the web sections, and defining non-dimensional parameters in Eq. 12, the circular bi-CTM's bending strain energy per unit length is given by Eq. 13.

$$\widehat{U} = \frac{UR_{1_O}^2}{h\left(D_{O_{11}}+D_{I_{11}}+D_{A_{11}}\right)}, \quad \widehat{\boldsymbol{D}}_{O,I,A} = \frac{\boldsymbol{D}_{O,I,A}}{D_{O_{11}}+D_{I_{11}}+D_{A_{11}}}, \quad \hat{C} = CR_{1_O} \tag{12}$$

$$\hat{U} = \frac{1}{h}\left[L_{1_O}\hat{k}_{1_O}^T\hat{D}_O\hat{k}_{1_O} + L_{2_O}\hat{k}_{2_O}^T\hat{D}_O\hat{k}_{2_O} + L_{1_I}\hat{k}_{1_I}^T\hat{D}_I\hat{k}_{1_I} + L_{2_I}\hat{k}_{2_I}^T\hat{D}_I\hat{k}_{2_I} + w\hat{k}_w^T(\hat{D}_O + \hat{D}_I + \hat{D}_A)\hat{k}_w\right] \tag{13}$$

D. Parabolic Bi-CTM Boom

The Bi-CTM can also have parabolic arcs instead of circular segments, which require a separate formulation of the strain energy equation. For manufacturability, only segment 1 is considered parabolic and segment 2 remains circular for both the outer and inner shells. The inextensional model's two parameter configuration requires the shell curvature to be a constant at any given energy state[13]. Since the curvature of a parabola does not satisfy this condition, the exact definition of the parabola cannot be used in the formulation. Instead, it is discretized into multiple circular arcs using biarc spline interpolation. A biarc is a pair of circular arcs having the same tangent vector at their connecting joint, and it is often used in curve fitting applications[25-27].

Given a bounded arbitrary function of monotonic curvature with one sign, a biarc was constructed by imposing geometric matching conditions at the two end points of the curve. With four matching conditions consisting of two end point locations and their tangents, there exists one free parameter of interpolating biarcs due to it having five degrees of freedom. Based on an error tolerance, this parameter, which determines the joint location of the two circular arcs, was searched iteratively with the bisection method until a suitable value and the resulting biarc was found. The error was defined as the maximum difference between the biarc and interpolated curve. If the specified accuracy was not achieved, the curve was subdivided into two equal segments, and the interpolation procedure was restarted on the first segment. The subdivision continues until the error requirement was met, and then the interpolation scheme resumes sequentially through all of the divided segments. Due to the geometric matching conditions imposed for each interpolating biarc, the entire circular spline approximating the curve retains tangent continuity. If the error tolerance is lowered, then the discretization density of the curve will increase. Since the parabola has non-monotonic curvature, only half of the curve was approximated with circular arcs and the other half is found with symmetry. Let the segment 1 parabola function be defined in Eq. 14, where the coefficient f is defined by the arc length L_p and the range $2y_j$ of the parabola using the arc length formula in Eq. 15.

$$p(y) = fy^2 \quad -y_j \leq y \leq y_j \tag{14}$$

$$L_p = 2\int_0^{y_j}\sqrt{1 + \left(\frac{dp}{dy}\right)^2}\,dy \tag{15}$$

If a common tangent is imposed between the bi-CTM's parabolic segment 1 and circular segment 2, and the parabola, web length w, and flattened height h are specified, then the radius R_2, subtended angle α_2, and arc length L_2 of segment 2 must be found, illustrated in Fig. 6 below.

Let any given circular arc in the interpolated parabola be denoted with the subscript $i = 1, ..., n$, where n is the total number of discretized arcs. Then (y_{p_n}, z_{p_n}), R_{p_n}, α_{p_n}, and L_{p_n} are the center coordinates, radius, subtended angle, and arc length of the last circular arc of the interpolated parabola in segment 1. (y_j, z_j) are the coordinates of the point shared by segments 1 and 2 and (y_2, z_2) are the center coordinates of the circular segment 2. All segment 1 parameters including y_j are known after interpolation, but z_j must be determined since the interpolated parabola is not yet aligned in the z-axis with segment 2.

To determine R_2, α_2, and z_j, the following relationships below can be derived from Fig. 6 where tangent continuity is imposed between the parabolic and circular segments. Eq. 17 yields α_2, then R_2 can be found with Eq. 16, which will then allow z_j in Eq. 18 to be found. Once z_j is known, the parabola is aligned with segment 2 to form the bi-CTM's cross section. For the strain energy equation, only the radii R_{p_i} and arc lengths L_{p_i} of the circular segments in the parabola are needed. However, the cross-sectional geometry derived here will be required to find the area moments of inertia and the bending stiffnesses, which will be presented in later sections.

$$h = 2(w + L_2) + L_p \tag{16}$$

$$y_j = y_{p_n} + R_{p_n}\sin\alpha_2 \tag{17}$$
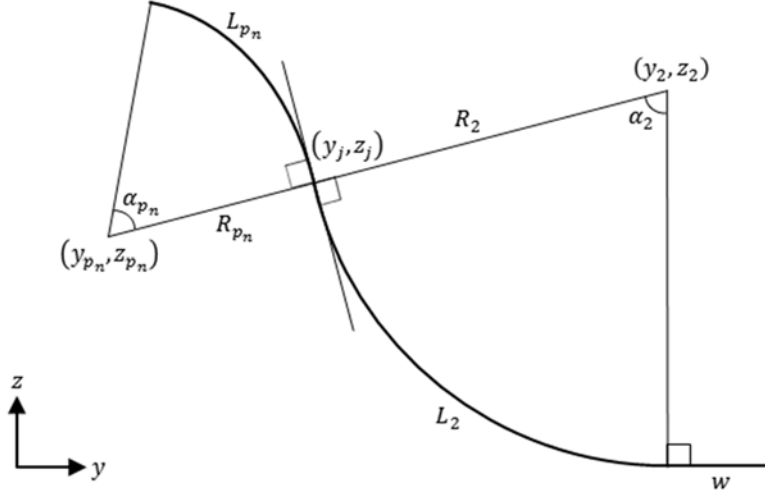
$$z_j = R_2(1 - \cos\alpha_2) \tag{18}$$

Fig. 6. Bi-CTM geometric parameters of the web, segment 2, and the last circular arc of the interpolated parabola in segment 1 on the right hand side of the outer shell.

In the parabolic segment 1, the circular arc curvatures resulting from the biarc interpolation will all have the same direction per shell. This means every arc in the parabola will have equal-sense bending for the outer shell and opposite-sense bending for the inner shell. The non-dimensional changes in curvature of segments 1 and 2 for both the outer and inner shells are given below.

$$\widehat{\boldsymbol{k}}_{p_{i_{O,I}}} = \frac{\hat{C}R_{p_{i_{O,I}}}}{2R_{p_{a_O}}} \begin{bmatrix} \pm(1-\cos 2\theta) \\ \cos 2\theta + 1 - \frac{2}{\hat{C}} \\ 2\sin 2\theta \end{bmatrix} \quad i = 1, \dots, n \tag{19}$$

$$\widehat{\boldsymbol{k}}_{2_{O,I}} = \frac{\hat{C}R_{2_{O,I}}}{2R_{p_{a_O}}} \begin{bmatrix} \mp(1-\cos 2\theta) \\ \cos 2\theta + 1 - \frac{2}{\hat{C}} \\ 2\sin 2\theta \end{bmatrix} \tag{20}$$

The changes in curvature of the web section is given by Eq. 5 and every shell segment is normalized by the mean radius of the outer shell's parabola $R_{p_{a_O}}$ with $\hat{C} = CR_{p_{a_O}}$, which is computed with the curvature $\kappa(y)$ and average value of a function in the formulas below.

$$\kappa(y) = \frac{\left|\frac{d^2 p}{dy^2}\right|}{\left[1+\left(\frac{dp}{dy}\right)^2\right]^{3/2}} \tag{21}$$

$$R_{p_{a_O}} = \frac{y_j}{\int_0^{y_j} \kappa(y)\,dy} \tag{22}$$

Assuming the outer and inner shell has the same segment 1 geometry, the parabolic bi-CTM's bending strain energy per unit length and its non-dimensional parameters are given below.

$$\widehat{U} = \frac{U R_{p_{a_O}}^2}{h(D_{O_{11}}+D_{I_{11}}+D_{A_{11}})}, \quad \widehat{\boldsymbol{D}}_{O,I,A} = \frac{D_{O,I,A}}{D_{O_{11}}+D_{I_{11}}+D_{A_{11}}}, \quad \hat{C} = CR_{p_{a_O}} \tag{23}$$

$$\widehat{U} = \frac{1}{h}\left[L_{2_O}\widehat{\boldsymbol{k}}_{2_O}^T\widehat{\boldsymbol{D}}_O\widehat{\boldsymbol{k}}_{2_O} + L_{2_I}\widehat{\boldsymbol{k}}_{2_I}^T\widehat{\boldsymbol{D}}_I\widehat{\boldsymbol{k}}_{2_I} + w\widehat{\boldsymbol{k}}_w^T(\widehat{\boldsymbol{D}}_O+\widehat{\boldsymbol{D}}_I+\widehat{\boldsymbol{D}}_A)\widehat{\boldsymbol{k}}_w + \frac{1}{2}\sum_{i=1}^n L_{p_{i_O}}\widehat{\boldsymbol{k}}_{p_{i_O}}^T\widehat{\boldsymbol{D}}_O\widehat{\boldsymbol{k}}_{p_{i_O}} + L_{p_{i_I}}\widehat{\boldsymbol{k}}_{p_{i_I}}^T\widehat{\boldsymbol{D}}_I\widehat{\boldsymbol{k}}_{p_{i_I}}\right] \tag{24}$$

For any of the two-shelled booms aforementioned, finding the energy minimizing equilibria involves taking the variation of $\widehat{U}$ with respect to the two configuration defining parameters, $\hat{C}$ and θ, as shown below

$$\delta \widehat{U} = \frac{\partial \widehat{U}}{\partial \theta} \delta \theta + \frac{\partial \widehat{U}}{\partial \hat{C}} \delta \hat{C} = 0 \tag{25}$$

To satisfy Eq. 25, it is necessary to impose the following conditions, whose solutions define the configurations under equilibrium:

$$\frac{\partial \widehat{U}}{\partial \theta} = 0, \quad \frac{\partial \widehat{U}}{\partial \hat{C}} = 0 \tag{26}$$

The stability of the solutions is determined by considering the non-dimensional stiffness matrix of the two-shelled boom in Eq. 27. The configuration is stable if $\widehat{K}$ is positive definite.

$$\widehat{K} = \begin{bmatrix} \frac{\partial^2 \widehat{U}}{\partial \theta^2} & \frac{\partial^2 \widehat{U}}{\partial \theta \partial \hat{C}} \\ \frac{\partial^2 \widehat{U}}{\partial \theta \partial \hat{C}} & \frac{\partial^2 \widehat{U}}{\partial \hat{C}^2} \end{bmatrix} \tag{27}$$

IV. Bistability Criterion

To determine which model parameters were critical for inducing bistability in two-shelled composite booms, a bistability criterion for each boom was derived. It also allows the direct evaluation of bistability without the need for minimizing the strain energy during parametric studies. Assuming no coupling between bending and twisting ($D_{16} = D_{26} = 0$) in either the outer or inner shell, there is a solution to the equilibrium equations in Eq. 26 at $\theta = \frac{\pi}{2}$ and boom type dependent $\hat{C}$. This corresponds to the coiled configuration of the second equilibrium position. The initial extended configuration of the first equilibrium position is always stable and at $\theta = 0$ and $\hat{C} = 1$. The bistability criterion is derived from checking if $\widehat{K}$ in Eq. 27 is positive definite for the second equilibrium position, which is done by evaluating the conditions below.

$$\frac{\partial^2 \widehat{U}}{\partial \theta^2} > 0, \quad \frac{\partial^2 \widehat{U}}{\partial \hat{C}^2} > 0, \quad \left(\frac{\partial^2 \widehat{U}}{\partial \hat{C}^2}\right)\left(\frac{\partial^2 \widehat{U}}{\partial \theta^2}\right) > \left(\frac{\partial^2 \widehat{U}}{\partial \theta \partial \hat{C}}\right)^2 \tag{28}$$

For every boom type, $\frac{\partial^2 \widehat{U}}{\partial \theta \partial \hat{C}}$ will be zero and $\frac{\partial^2 \widehat{U}}{\partial \hat{C}^2}$ will always be positive, though the exact equation will vary due to differences in the non-dimensional strain energy per unit length equations. Therefore, the second equilibrium position will be stable and the boom will be bistable if $\frac{\partial^2 \widehat{U}}{\partial \theta^2} > 0$ is satisfied.

A. Bi-SHEARLESS Boom
The Bi-SHEARLESS boom's $\hat{C}$ at $\theta = \frac{\pi}{2}$, $\frac{\partial^2 \widehat{U}}{\partial \hat{C}^2}$, and bistability criterion are given below. The non-dimensional curvature of the coiled state and the bistability criterion only depend on the individual components of the $\widehat{\boldsymbol{D}}_{O,I}$ matrices, or the bending stiffnesses of the outer and inner shells.

$$\hat{C} = \frac{\widehat{D}_{O_{12}} - \widehat{D}_{I_{12}}}{\widehat{D}_{O_{11}} + \widehat{D}_{I_{11}}} \tag{29}$$

$$\frac{\partial^2 \widehat{U}}{\partial \hat{C}^2} = \widehat{D}_{O_{11}} + \widehat{D}_{I_{11}} \tag{30}$$

$$\frac{\partial^2 \widehat{U}}{\partial \theta^2} = \frac{2(\widehat{D}_{I_{12}} - \widehat{D}_{O_{12}})}{(\widehat{D}_{O_{11}} + \widehat{D}_{I_{11}})^2}\left[(\widehat{D}_{O_{11}} + \widehat{D}_{I_{11}})(\widehat{D}_{O_{22}} + \widehat{D}_{I_{22}}) + 2\widehat{D}_{I_{12}}\left(\widehat{D}_{I_{66}} + \widehat{D}_{O_{12}} + \widehat{D}_{O_{66}} - \frac{1}{2}\widehat{D}_{I_{12}}\right) - 2\widehat{D}_{O_{12}}\left(\widehat{D}_{I_{66}} + \widehat{D}_{O_{66}} + \frac{1}{2}\widehat{D}_{O_{12}}\right)\right] > 0 \tag{31}$$

Therefore, the second equilibrium point will be stable and the Bi-SHEARLESS boom will be bistable if Eq. 31 is satisfied.

B. Bi-TRAC and Bi-X Boom

The Bi-TRAC and Bi-X booms' $\hat{C}$ at $\theta = \frac{\pi}{2}$, $\frac{\partial^2 \hat{U}}{\partial \hat{C}^2}$, and bistability criterion are given below. In addition to the bending stiffnesses, the non-dimensional curvature of the coiled state and the bistability criterion now also depend on the boom's cross-sectional geometry, which are the flattened height, h, and web length, w.

$$\hat{C} = \frac{(h-w)(\hat{D}_{I_{12}} - \hat{D}_{O_{12}})}{h(\hat{D}_{O_{11}} + \hat{D}_{I_{11}}) + w\hat{D}_{A_{11}}} \tag{32}$$

$$\frac{\partial^2 \hat{U}}{\partial \hat{C}^2} = \hat{D}_{O_{11}} + \hat{D}_{I_{11}} + \frac{w}{h}\hat{D}_{A_{11}} \tag{33}$$

$$\frac{\partial^2 \hat{U}}{\partial \theta^2} = \frac{2(\hat{D}_{O_{12}} - \hat{D}_{I_{12}})(h-w)^2}{h(h(\hat{D}_{O_{11}} + \hat{D}_{I_{11}}) + w\hat{D}_{A_{11}})^2}\Big[h\big[(\hat{D}_{O_{11}} + \hat{D}_{I_{11}})(\hat{D}_{O_{22}} + \hat{D}_{I_{22}}) - 2\hat{D}_{I_{12}}\big(\hat{D}_{I_{66}} + \hat{D}_{O_{66}} + \frac{1}{2}\hat{D}_{I_{12}}\big) + 2\hat{D}_{O_{12}}\big(\hat{D}_{I_{12}} + \hat{D}_{I_{66}} + \hat{D}_{O_{66}} - \frac{1}{2}\hat{D}_{O_{12}}\big)\big] +$$
$$w\big[\hat{D}_{I_{12}}(\hat{D}_{I_{12}} - 2\hat{D}_{A_{66}} - 2\hat{D}_{O_{12}}) + \hat{D}_{O_{12}}(\hat{D}_{O_{12}} + 2\hat{D}_{A_{66}}) + \hat{D}_{A_{11}}(\hat{D}_{I_{22}} + \hat{D}_{O_{22}})\big]\Big] > 0 \tag{34}$$

C. Bi-CTM Boom

The circular Bi-CTM boom's $\hat{C}$ at $\frac{\pi}{2}$, $\frac{\partial^2 \hat{U}}{\partial \hat{C}^2}$, and bistability criterion are given below in terms of the parameters listed in Eq. 38 for simplification. Note that the radius of every segment is normalized by R_{1_O} and this is denoted with a hat (e.g. $\hat{R}_{2_O} = R_{2_O}/R_{1_O}$). The non-dimensional curvature of the coiled state and the bistability criterion now depend on the arc lengths and radii of every circular segment, and web length, in addition to the bending stiffnesses of both shells.

$$\hat{C} = \frac{\hat{D}_{O_{12}}E_2 - \hat{D}_{I_{12}}F_2}{\hat{D}_{O_{11}}(E_1 + w) + \hat{D}_{I_{11}}(F_1 + w) + w\hat{D}_{A_{11}}} \tag{35}$$

$$\frac{\partial^2 \hat{U}}{\partial \hat{C}^2} = \frac{2}{h}\big[\hat{D}_{O_{11}}(E_1 + w) + \hat{D}_{I_{11}}(F_1 + w) + w\hat{D}_{A_{11}}\big] \tag{36}$$

$$\frac{\partial^2 \hat{U}}{\partial \theta^2} = \frac{4(\hat{D}_{I_{12}}F_2 - \hat{D}_{O_{12}}E_2)}{h(\hat{D}_{O_{11}}(E_1 + w) + \hat{D}_{I_{11}}(F_1 + w) + w\hat{D}_{A_{11}})^2}\Big[\hat{D}_{O_{11}}\hat{D}_{O_{22}}E_1(E_1 + w) - \hat{D}_{I_{12}}{}^2F_2{}^2 - \hat{D}_{O_{12}}{}^2E_2{}^2 - 2\hat{D}_{O_{12}}\hat{D}_{O_{66}}E_2(E_1 + w) + \hat{D}_{I_{11}}\hat{D}_{I_{22}}F_1(F_1 + w) +$$
$$2\hat{D}_{I_{12}}\hat{D}_{I_{66}}F_2(F_1 + w) + \hat{D}_{I_{11}}\hat{D}_{O_{22}}(E_1 w + H_1 + G_1) - 2\hat{D}_{O_{12}}\hat{D}_{I_{66}}(E_2 w + H_1 - G_1) + 2\hat{D}_{I_{12}}\hat{D}_{O_{12}}(H_2 - G_2) + \hat{D}_{I_{22}}\hat{D}_{O_{11}}(H_1 + F_1 w + G_1) +$$
$$2\hat{D}_{I_{12}}\hat{D}_{O_{66}}(H_2 + F_2 w + G_2) + w\big(\hat{D}_{A_{11}}\hat{D}_{O_{22}}E_1 - 2\hat{D}_{A_{66}}\hat{D}_{O_{12}}E_2 + \hat{D}_{A_{11}}\hat{D}_{I_{22}}F_1 + 2\hat{D}_{A_{66}}\hat{D}_{I_{12}}F_2\big)\Big] > 0 \tag{37}$$

$$E_{1,2} = L_{1_O} \pm L_{2_O}\hat{R}_{2_O}^2, \quad F_{1,2} = L_{1_I}\hat{R}_{1_I}^2 \pm L_{2_I}\hat{R}_{2_I}^2, \quad G_{1,2} = L_{2_O}\hat{R}_{2_O}^2\big(L_{1_I}\hat{R}_{1_I}^2 \pm L_{2_I}\hat{R}_{2_I}^2\big), \quad H_{1,2} = L_{1_O}(L_{1_I}\hat{R}_{1_I}^2 \pm L_{2_I}\hat{R}_{2_I}^2) \tag{38}$$

The criterion for the parabolic Bi-CTM is not found because it depends on the number of discretizations in the biarc interpolation of the parabolic segment 1. This means the criterion will change every time the parabola or the error tolerance is altered, which prevents it from being useful for parametric studies on bistability. In addition, the computational cost of deriving the criterion is greater than any of the other boom types, especially when the number of discretizations is high. As an alternative, the criterion for the circular Bi-CTM can be used as a rough approximation of the parabolic Bi-CTM criterion.

V. Other Boom Parameters for Evaluation

A. Deployment Force

With the strain energy solutions of the stable coiled configurations identified for the two-shelled composite booms, the self-deployment force of the booms can now be found. Neglecting the effects of friction, creep, and hysteresis of the composite shells, the ideal deployment force, F, of any boom type is simply their dimensional bending strain energy per unit length, U, in the second equilibrium position corresponding to the coiled configuration, where $\theta = \frac{\pi}{2}$ and $\hat{C}$ is boom type dependent[28].

$$F = U\left(\frac{\pi}{2}, \hat{C}\right) \tag{39}$$

B. Allowable Length According to Volume Requirement

An important boom design consideration is the allowable length, which is dictated by the packaged volume requirement while stowed and the coiled diameter at the onset of wrap instability. When the booms are coiled about themselves, the curvature $\hat{C}$ decreases until the strain energy state is no longer in the secondary stable configuration. As the outer radius of the coil, r_f, increases from wrapping, the minimum strain energy path will approach unstable saddle point configurations, that satisfy Eq. 26 but not Eq. 28, which will result in warping of the boom coil. This instability will prevent the boom from being self-contained, which is a key advantage of bistable booms. The length limit where bistability is lost is found with the equations for the outer radius of the coil, r_f, the total thickness of all booms coiled, t_t, and the total number of wraps in the coil, w_c, as given below. r_i is the initial coiled radius, which is assumed here to be the radius $1/C$ of the secondary stable state, n_b is the total number of two-shelled booms coiled per spool, μ is the packaging efficiency, L is the boom length, and $t_{O,I,A}$ are the thicknesses of the outer shell, inner shell, and the adhesive, respectively.

$$r_f = r_i + w_c t_t \tag{40}$$

$$t_t = n_b(t_O + t_I + t_A)(1 + \mu) \tag{41}$$

$$w_c = \sqrt{\left(\frac{r_i}{t_t}\right)^2 + \frac{L}{\pi t_t}} - \frac{r_i}{t_t} \tag{42}$$

By setting r_f as the coiled radius of the unstable saddle points, the length limit where the boom is no longer bistable is found by substituting Eq. 41 and Eq. 42 into Eq. 40 and solving for the boom length L. r_f can also be set to the maximum allowable radius according to the packaged volume system requirement to find the allowable boom length.

C. Area Moments of Inertia and Torsional Constant

Besides evaluating the stability of two-shelled composite booms, determining their area moments of inertia about the principal axes, I_{yy} and I_{zz}, and torsional constant, J, is critical for fulfilling system requirements for bending and torsional stiffnesses. Optimal cross sectional geometries of the boom that maximize these metrics, and therefore the stiffnesses, are obtained through parametric analysis. The effective elastic and shear modulus of the boom will not be considered since they only depend on the thin-ply material properties and laminates. In the extended configuration, the booms were oriented as shown in Fig. 1. The geometric center of the cross sections for the bi-SHEARLESS, bi-X, and bi-CTM booms were placed at the origin of the $y - z$ coordinate system. For the bi-TRAC, the origin was placed at the joint between the web and the flanges. Based on relevant geometric parameters such as the radii and lengths of circular arcs, flattened height, web length, and subtended angles, each boom's cross section was discretized into the (y, z) coordinates with simple trigonometry. Thus, each segment consisting of a pair of (y, z) coordinates was then idealized as a rectangle rotated about the origin by θ. The area moments of inertia of every segment about their own centroid relative to the y and z axes, I_{y_j} and I_{z_j}, were found with the following equations. Let any given rectangular segment be denoted with the subscript $j = 1, ..., m$, where m is the total number of segments. l_j and t_j are the length and thickness of each segment.

$$I_{y_j} = \frac{1}{12} l_j t_j (l_j^2 \sin^2 \theta + t_j^2 \cos^2 \theta) \tag{43}$$

$$I_{z_j} = \frac{1}{12} l_j t_j (l_j^2 \cos^2 \theta + t_j^2 \sin^2 \theta) \tag{44}$$

The boom's area moments of inertia can be found by summing I_{y_j} or I_{z_j} through the parallel axis theorem, as shown below. A_j is the area of each segment and d_j is the distance from each segment's centroid to the y or z axis.

$$I_{yy,zz} = \sum_{j=1}^{m} I_{y,z_j} + A_j d_j^2 \tag{45}$$

The torsional constant of each boom is found by summing the torsional constants of each segment in open sections, J_O, and closed sections, J_C, as shown below. A_E is the total enclosed area in the closed section.

$$J_O = \sum_{j=1}^{m} \frac{1}{3} l_j t_j{}^3 \qquad (46)$$

$$J_C = 4A_E{}^2 / \sum_{j=1}^{m} \frac{l_j}{t_j} \qquad (47)$$

For the Bi-TRAC and Bi-X booms, Eq. 46 is used since these booms consist only of open section segments. The Bi-CTM boom's torsional constant is the sum of Eq. 46 and 47 because it consists of both open and closed sections, corresponding to the web and circular segments. The Bi-SHEARLESS boom should be considered as an open section structure for conservatism, and so Eq. 46 was used to find its torsional constant. This is due to each shell's tendency to twist independently while the boom is under torsion as the sleeve provides a limited amount of coupling[14]. In reality, the friction between the shells and the sleeve results in a structure that is torsionally stiffer than what Eq. 46 yields. Therefore, Eq. 46 is considered as the worst case lower bound limit of the torsional constant. Although the approach presented above only yields an approximation of J, I_{yy}, and I_{zz}, it is versatile, and can accommodate every boom type discussed in this paper regardless of any geometric variations.

VI. Analytical Model Validation with Case Studies

With the inextensional analytical model established for each two-shelled bistable boom type, case studies for the Bi-SHEARLESS and Bi-TRAC are presented based on specimens already manufactured and characterized[14]. These preliminary cases serve as limited verification for the model's stable solutions since the other boom types have not been completed yet, and they will only be analytically evaluated in the parametric design studies. Table 1 shows the material description and properties of the thin-ply composites and adhesive used for fabricating the shells in the deployable booms[14]. Table 2 and 3 summarize two-shelled booms and the corresponding analytical model and experimental results.

Table 1. Material properties of thin-ply composites and adhesive

Label	Material Description	Fiber/Resin	E_1 (GPa)	E_2 (GPa)	v_{12}	G_{12} (GPa)	Lamina AW (g/m^2)	Thickness t (mm)
C	Intermediate Modulus (IM) Unidirectional (UD) Carbon Fiber	MR60H/PMT-F7	164	8.55	0.274	3.51	56	0.0374
PW$_C$	Plain Weave IM Carbon Fiber	HTA40/PMT-F7	76.5	76.5	0.031	3.79	90	0.0635
PW$_{AQ}$	Plain Weave Astroquartz II	AstroQuartz/PMT-F7	24.5	24.5	0.069	3.97	93	0.0533
BR$_C$	Braid IM Carbon Fiber	T300-1K/PMT-F7	74.7	74.7	0.027	5.57	125	0.0677
G	Unidirectional (UD) Glass Fiber	S2-Glass/PMT-F7	56.4	12.8	0.285	3.9	100	0.0514
CHM	High Modulus UD Carbon Fiber	HS40/PMT-F7	273.1	9.09	0.268	3.88	42	0.0261
A	Hysol EA9628 Film Epoxy	N/A	2.136	2.136	0.712	0.624	146	0.1

Table 2. Inextensional model results comparison to experimental data for select TRAC and SHEARLESS booms.

Boom version	Inner Shell Laminate	Outer Shell Laminate	Exp. Bi-stable	Model Bi-stable	Bistability Criterion Value	Exp. Wrap Diameter (mm)	Stable Model Diameter (mm)	Diameter Percent Error (%)
TRAC								
v13	[0$_G$/45PW$_C$/0$_G$]	[45PW$_{AQ}$/0$_C$/45PW$_{AQ}$]	No	No	-0.0001	55.00	N/A	N/A
v15	[45PW$_C$/0$_C$/45PW$_C$]	[0-90PW$_C$]	Yes	Yes	0.0311	72.00	82.10	14.03
v16	[45PW$_C$/0$_C$/45PW$_C$]	[0$_C$/45PW$_C$]	Yes	Yes	0.0244	79.00	102.82	30.15
v17	[45PW$_C$/0$_C$/45PW$_C$]	[0$_G$/45BR$_C$]	Yes	Yes	0.0219	70.00	118.33	69.05
SHEARLESS								
v3	[45PW$_C$/0$_C$/45PW$_C$]	[45PW$_C$/0$_C$/45PW$_C$]	No	No	0.0000	40.53	N/A	N/A
v4	[0-90PW$_C$]	[45PW$_C$/0$_C$/45PW$_C$]	Yes	Yes	0.0163	38.00	44.70	17.63
v5	[45PW$_C$/0$_C$]	[45PW$_C$/0$_C$/45PW$_C$]	Yes	Yes	0.0068	64.00	56.00	12.50
v6	[45BR$_C$/0$_C$]	[45PW$_C$/0$_C$/45PW$_C$]	Yes	Yes	0.0048	65.00	59.58	8.34
v7	[45PW$_{AQ}$/0$_C$/45PW$_{AQ}$]	[45PW$_C$/0$_C$/45PW$_C$]	Yes	Yes	0.0019	71.00	63.53	10.52
v8	[45PW$_{AQ}$/0$_C$/45PW$_{AQ}$]	[45BR$_C$/0$_C$/45BR$_C$]	Yes	Yes	0.0003	75.00	66.44	11.41

Table 3. Design metric results for select TRAC and SHEARLESS booms.

Boom version	Exp. Length Allowed – 2 Co-reeled Booms (m)	Model Length Allowed – 2 Co-reeled Booms (m)	Bistability Limit Length – 1 Boom (m)	Deployment Force (N)	I_{yy} (mm^4)	I_{zz} (mm^4)	J (mm^4)
TRAC							
v13	4.48-3.82	N/A	N/A	N/A	3267.50	2314.60	0.21
v15	3.61-3.00	2.66	9.67	0.29	2752.00	1886.60	0.15
v16	2.40-2.04	Exceeds Limit (EL)	6.32	0.35	2990.50	2081.30	0.17
v17	3.24-2.77	Exceeds Limit (EL)	1.17	0.43	3098.50	2174.10	0.18
SHEARLESS							
v3	6.66	N/A	N/A	N/A	1342.00	1676.50	0.13
v4	7.41	8.71	3.52	0.72	781.47	1162.00	0.07
v5	4.40	6.48	2.40	0.95	1032.20	1352.70	0.08
v6	4.16	5.97	1.89	1.02	1056.50	1374.10	0.08
v7	3.17	4.88	0.80	1.29	1254.30	1572.40	0.11
v8	2.55	4.43	0.12	1.52	1284.30	1615.30	0.12

The PW and BR labels in the layups denote plain weave and braid fabrics while ply orientations without a following label denote unidirectional plies. The C, G, and AQ subscripts denote carbon fiber, glass fiber, and astroquartz materials, respectively. These thin-ply composite materials were chosen to comply with stringent thickness and areal weight requirements of space missions, with cured ply thicknesses below 0.065 mm for unidirectional materials and double that for textile fabrics. The adhesive used for bonding the two shells of all booms containing web sections was Hysol EA 9628 epoxy film. The SHEARLESS and TRAC booms had an initial, as-manufactured, extended radius of 16 mm and 25.4 mm for both shells, respectively. Both boom types have a flattened height of 45 mm and the TRAC booms have a web width of 6 mm.

According to Table 2, the inextensional model successfully predicted bistability with the criteria listed in Eq. 31 and Eq. 34, and there was fairly good agreement for the coiled diameter compared to the experimental measurements. The exception was the Bi-TRAC v17 boom, which may be due to manufacturing or measurement errors. The over-prediction of Bi-TRAC coiled diameters was due to the model's inextensional assumption, which artificially increased the booms' stiffnesses restricting bending. The Bi-SHEARLESS results were under-predicted by the model and had lower errors because of the neglection of the friction strain energy from the coupled interaction between the shells and the sleeve. The model may over-predict the coiled diameter as seen for the Bi-TRAC booms. However, the inextensional model is able to distinguish between monostable and bistable two-shelled booms.

According to Ref. 14, the stowed volume requirement for the NEA Scout solar sail mission on a 6U CubeSat is 97 mm for the maximum outer diameter of two co-reeled booms ($n_b = 2$) that have a flattened height of 45 mm. Since this applies to both the Bi-SHEARLESS and Bi-TRAC booms, an r_f (outer radius of coil) value of 48.5 mm from Eq. 40 was used for computing their allowable lengths according to volume requirements. As seen in Table 3, the under-prediction of Bi-SHEARLESS coiled diameters resulted in the over-prediction of allowable lengths and vice versa for the Bi-TRAC booms, which reveals that the errors of these two metrics were correlated. Table 3 also shows the maximum length allowed for a single boom $n_b = 1$ before it reached a diameter corresponding to an unstable saddle point, which wass assumed to be the initiation of warping of the coiled boom, and the loss of bistability.

For the purpose of evaluating the equilibrium states using the inextensional model, polar contour plots of the non-dimensional strain energy per unit length as a function of $\hat{C}$ and θ for the Bi-SHEARLESS v4 and Bi-TRAC v15 booms are presented in Fig. 7. These booms have four equilibrium positions, each corresponding to an energy minimum, where the first stable point was the initially, as-manufactured, extended configuration at $\hat{C} = 1$ and $\theta = 0$. For the Bi-SHEARLESS_v4 boom, the second stable configuration was found in the coiled state at $\theta = \pi/2$ and $\hat{C} = 0.716$, which corresponds to a coiled diameter of 44.70 mm. This was in fairly good agreement with the experimentally measured coiled diameter of 38 mm, with an error of 17.6%. For the Bi-TRAC_v15 boom, the coiled stable state at $\theta = \pi/2$ and $\hat{C} = 0.619$ resulted in a coiled diameter of 82.1 mm, with an error of 14.0% when compared to the experimental diameter of 72 mm. It should be noted that the measured values slightly vary each time it is coiled, so the percent errors could fluctuate. The third and fourth equilibrium positions of both plots in Fig. 7 are unstable saddle points located between the coiled and extended configurations, and are not explored any further. The strain energy distributions are qualitatively consistent between all bistable booms, regardless of their type.
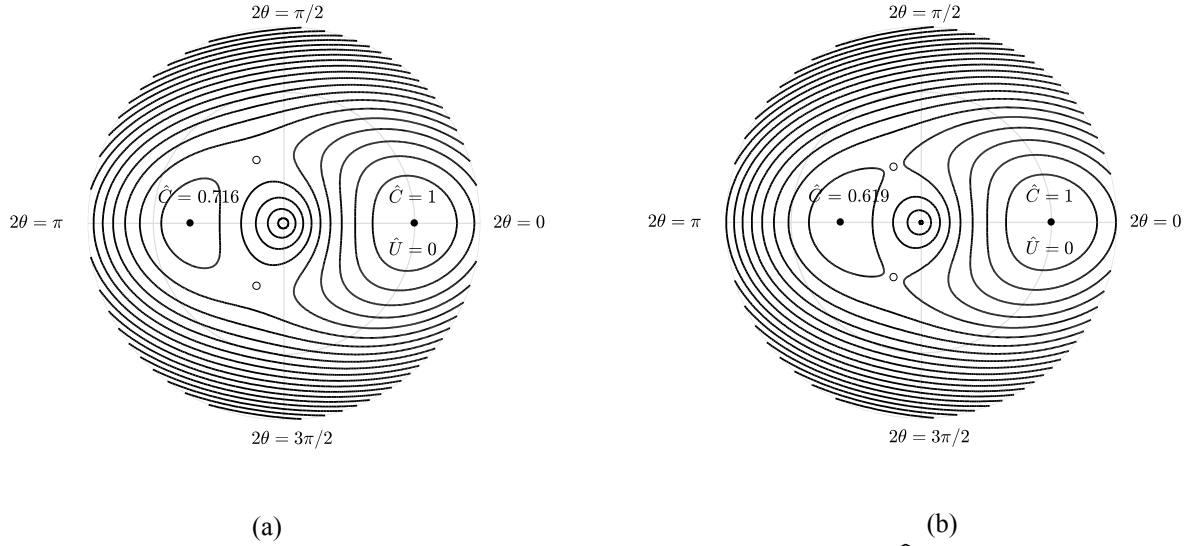
(a)   (b)

Fig. 7. Polar contour plot of the non-dimensional bending strain energy per unit length, $\widehat{U}$, as a function of the non-dimensional coiled curvature, $\widehat{C}$, and the angle of the shell relative to an underlying cylinder, θ, for (a) Bi-SHEARLESS_v4, and (b) Bi-TRAC_v15 booms. The two stable locations are marked as dots while the two unstable points are marked as circles. The contour lines are separated by a constant $\Delta\widehat{U} = 0.05$.

VII.   Parametric Analysis

The optimal cross section of each boom type can be obtained by maximizing the area moments of inertia and the torsional constant while maintaining bistability and meeting system requirements for the allowable length (volume) and the deployment force. The objective is to maximize I_{yy}, I_{zz}, and J while varying relevant geometric parameters of the cross-section and maintaining a positive $\frac{\partial^2 \widehat{U}}{\partial\theta^2}$ value to ensure that the booms remain bistable. While the deployment force is not considered in the parametric analysis, it can be used to filter out data points that do not meet the associated system requirements. For the layup of the boom, the bistable [45PW$_C$/0$_C$/45PW$_C$] laminate was used for the shell bending in the equal-sense direction, which was the outer shell for the Bi-SHEARLESS and Bi-CTM booms, and the inner shell for the Bi-TRAC and Bi-X booms. The monostable [0-90PW$_C$] laminate was used for the shell bending in the opposite-sense direction, or the shell opposite to the ones mentioned previously for each boom type.

These layups were chosen for all parametric studies since preliminary experimental and analytical data show that this combination of shells most easily introduces a second stable state out of all the layups investigated until now. This is evidenced by their lowest coiled diameters and highest positive bistability criterion value. Since the volume-constrained allowable length depends on the shell thicknesses determined by their layup and materials, all investigated cross-sectional geometries should yield identical allowable lengths for the same initial coiled radius. Therefore, mission requirements for stowed volume were not accounted for in the parametric analysis. Finally, although the extended inextensional model introduced allows for different inner and outer shell cross-sectional geometries, the work presented in this section assumes that they were identical for simplicity. The geometric parameters were not differentiated between the inner and outer shells and were varied equally.

A. Bi-SHEARLESS, Bi-TRAC, and Bi-X Booms
For the Bi-SHEARLESS boom, the only cross-sectional parameter that can be varied is the subtended angle or the radius of the inner and outer shells since they are dependent on each other. With stowed volume requirements in Ref. 14 requiring a flattened height of 45 mm, the subtended angle was varied from 10° to 180° with a 1 degree step size corresponding to a radius of 128.9 mm to 14.3 mm. For the Bi-TRAC and Bi-X booms, the flattened height was still 45 mm, but the web width was 6 mm and the subtended angle was varied from 10° to 90° with a 1 degree step size, corresponding to a radius of 223.4 mm to 24.8 mm for the Bi-TRAC and 111.7 mm to 12.4 mm for the Bi-X booms. The variation of these cross-sectional parameters are visualized in Fig. 8.

Since the bistability criteria in Eq. 31 and Eq. 34 do not depend on the subtended angles or the radii of the shells, their layup will ensure that all geometries in the parametric analysis will be bistable.
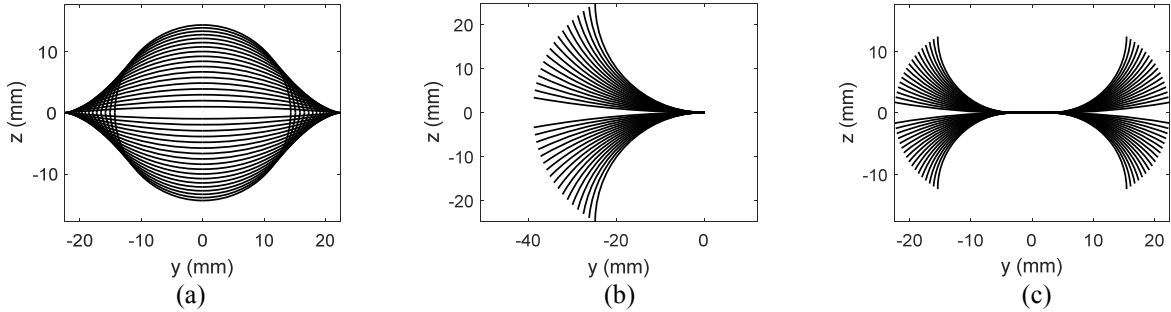
Fig. 8. Varying cross-sections in parametric analysis for (a) Bi-SHEARLESS, (b) Bi-TRAC, and (c) Bi-X booms.

Figure 9 shows how the area moments of inertia I_{yy}, I_{zz}, and torsional constant J varies with the subtended angles and radii of the shells for the Bi-SHEARLESS boom. As the subtended angle increases and the radius decreases, the cross-sectional curvature rises and this results in I_{yy} increasing and I_{zz} decreasing. Since the extended boom must be able to withstand loads in both the y and z directions during operation, the optimal cross-sectional geometry is that which yields the maximum value for the area moment of inertia that is the lower of the two directions, which is I_{yy}. This ensures that the boom will retain adequate bending stiffness regardless of the load direction. The cross-section with the maximum subtended angle of 180° and minimum radius of 14.3 mm was optimal and resulted in I_{yy} of 885 mm^4, I_{zz} of 1052 mm^4, and J of 0.0704902 mm^4. Since the torsional constant remains consistent over the parameters, it is not considered when determining the optimal boom geometry.
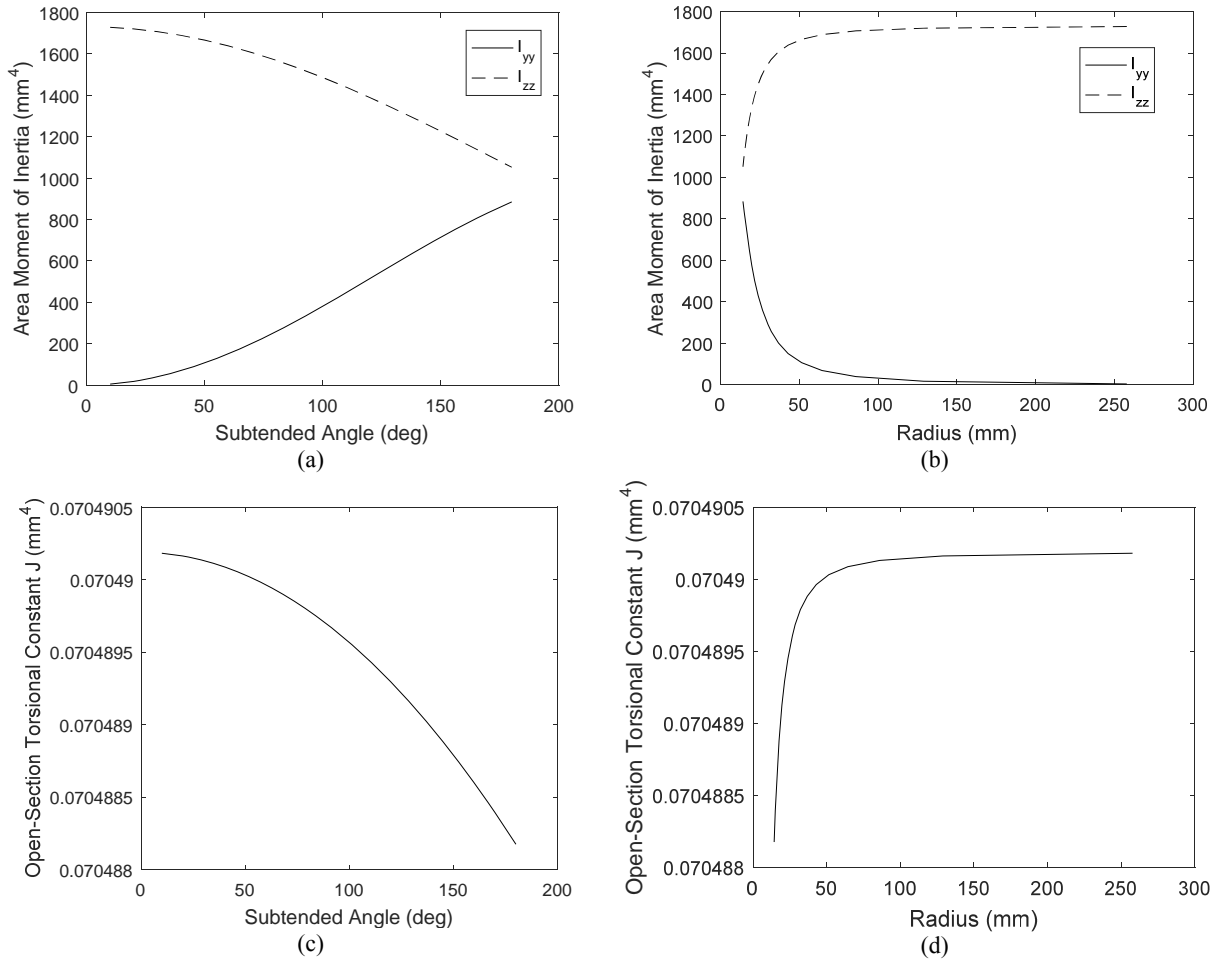

Fig. 9. Bi-SHEARLESS parametric analysis on area moments of inertia vs. (a) subtended angle and (b) radius, and torsional constant vs. (c) subtended angle and (d) radius.

15
American Institute of Aeronautics and Astronautics

Fig. 10 shows the variation of the area moments of inertia and torsional constant against the subtended angle and radius of the Bi-TRAC boom. Unlike the Bi-SHEARLESS boom, I_{yy} and I_{zz} cross each other as the subtended angle increases and the radius decreases. Instead of selecting the maximum value of the lower area moment of inertia, the optimal cross-section is where I_{yy} and I_{zz} meet, which ensures that the boom will have consistent bending stiffnesses in any direction. According to Fig. 10, this corresponds to a subtended angle of 78° and radius of 28.6 mm that yields 2238 mm^4 for both I_{yy} and I_{zz} and 0.146 mm^4 for J. However, the cross-sectional geometry that yields the maximum torsional constant was when the subtended angle is 90° and the radius is 24.8 mm. The torsional constant significantly varies and so this metric must be taken into account. The optimal cross section must be chosen based on whether the bending or torsional stiffnesses are prioritized, as either selection will sacrifice stiffness in some form.
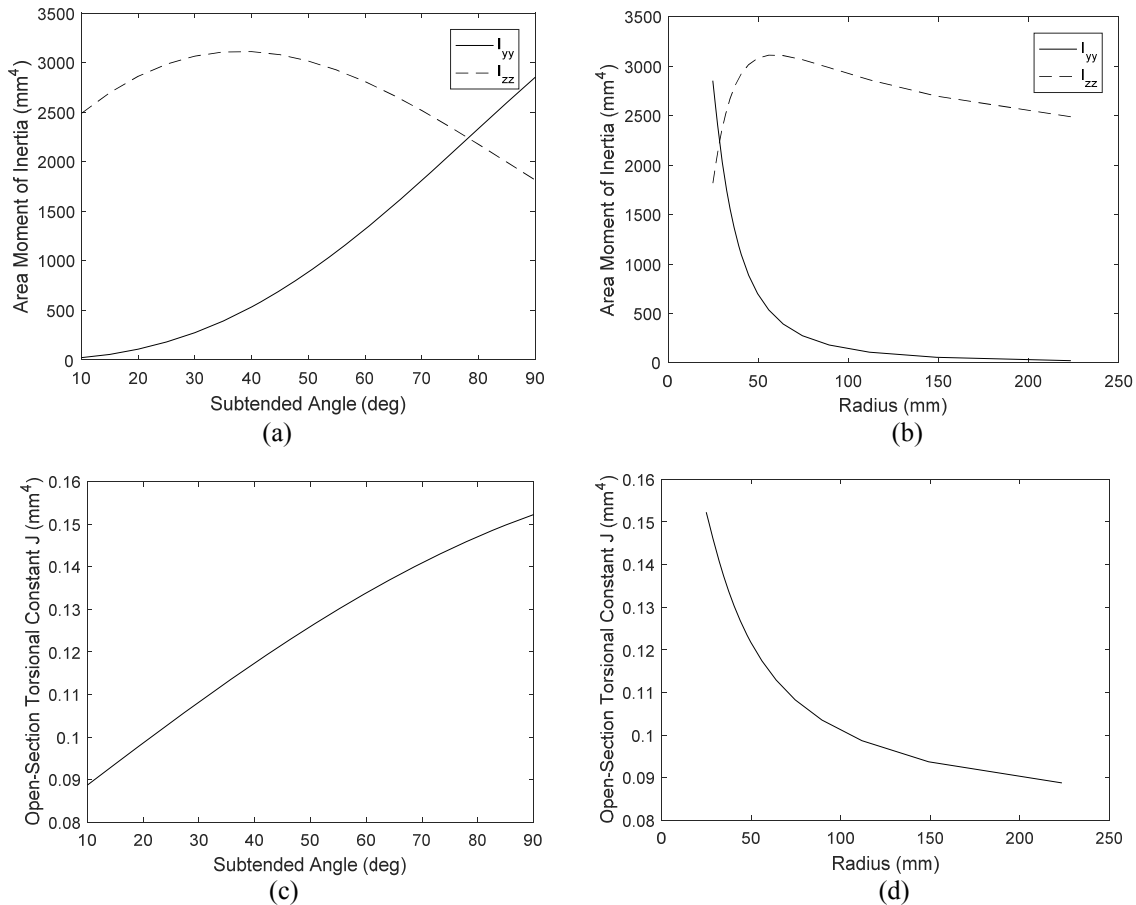
Fig. 10. Bi-TRAC parametric analysis on area moments of inertia vs. (a) subtended angle and (b) radius, and torsional constant vs. (c) subtended angle and (d) radius.

Fig. 11 shows the variation of the area moments of inertia and torsional constant with the subtended angle and radius of the Bi-X boom. Unlike the Bi-TRAC boom, I_{yy} and I_{zz} never cross each other and so the optimal cross section is selected on the same basis as the Bi-SHEARLESS boom. The subtended angle of 90° and radius of 12.4 mm are when both moments of inertia are maximized, and yields 498 mm^4 for I_{yy} and 1885 mm^4 for I_{zz}. This cross section is also the optimal choice for maximizing the torsional constant, which is 0.103 mm^4. This means there are no competing designs tied with each metric like the Bi-TRAC boom. When comparing the boom types covered until now, the Bi-TRAC boom retains the highest area moments of inertia and torsional constant at its optimal cross-sectional geometry, while the optimized Bi-SHEARLESS boom has the lowest out-of-plane bending and torsional stiffnesses and the optimized Bi-X boom has the lowest in-plane bending stiffness.
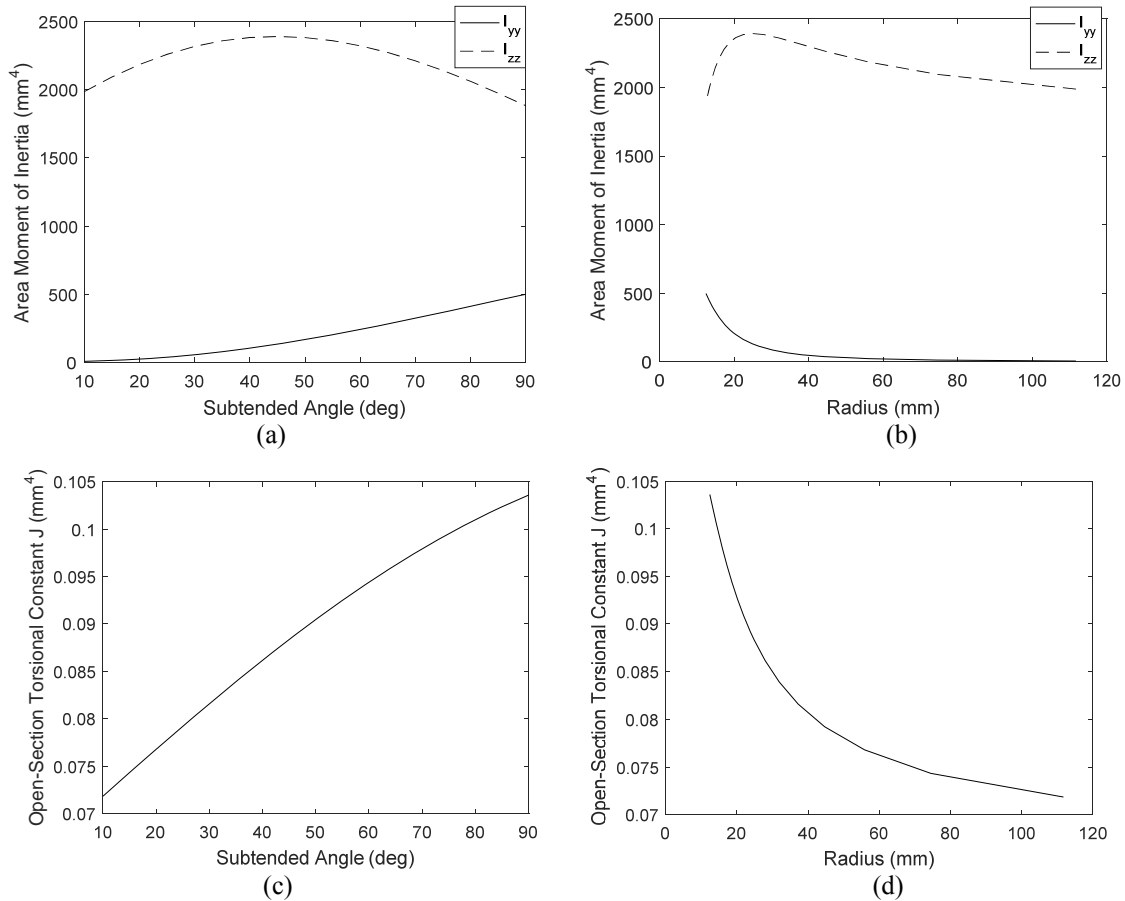
Fig. 11. Bi-X boom parametric analysis on area moments of inertia vs. (a) subtended angle and (b) radius, and torsional constant vs. (c) subtended angle and (d) radius.

B. Circular Bi-CTM Boom

The circular Bi-CTM boom has two independent parameters that can be varied, and these are the subtended angle of both circular segments and the radius of either segment. Note that in order to prevent kinks between the arcs and maintain tangent continuity, the subtended angle of both segments must be identical. If a radius is specified for one arc, then the other segment radius is set and cannot be altered. All Bi-CTM booms have a flattened height of 110 mm with a web width of 4 mm per side, as determined by the boom requirements[24]. In the parametric analysis, the subtended angle was varied from 10° to 85° with a 2.5 degree step size and those limits were set by manufacturing constraints. The segment 1 radius was varied from 6.25 mm to 285.96 mm, where 6.25 mm was a manufacturing limitation and 285.96 mm was the upper limit determined by the total arc length of segments 1 and 2, being 51 mm. This range corresponds to the radius of segment 2 being varied from 285.96 mm to 6.25 mm. Segment 1 and 2 are interchangeable in the parametric analysis, and the results will be identical regardless of which radius is varied. In practice, the upper limit was set to 306.25 mm so that an increment size of 10 mm can be implemented and any points with a resulting radius of less than 6.25 mm were filtered out. Since the bistability criterion in Eq. 37 and 38 depends on the radii of the circular segments, it was applied for every cross-sectional configuration and all monostable points were also filtered out. This means that, aside from the shell laminates, the shell geometry also plays a critical role in yielding bistable designs. Figure 12 shows the circular Bi-CTM area moments of inertia and torsional constant against the variation of subtended angles and radii of the segments for both shells.

American Institute of Aeronautics and Astronautics

(a)

(b)

(c)

(d)

(e)

(f)
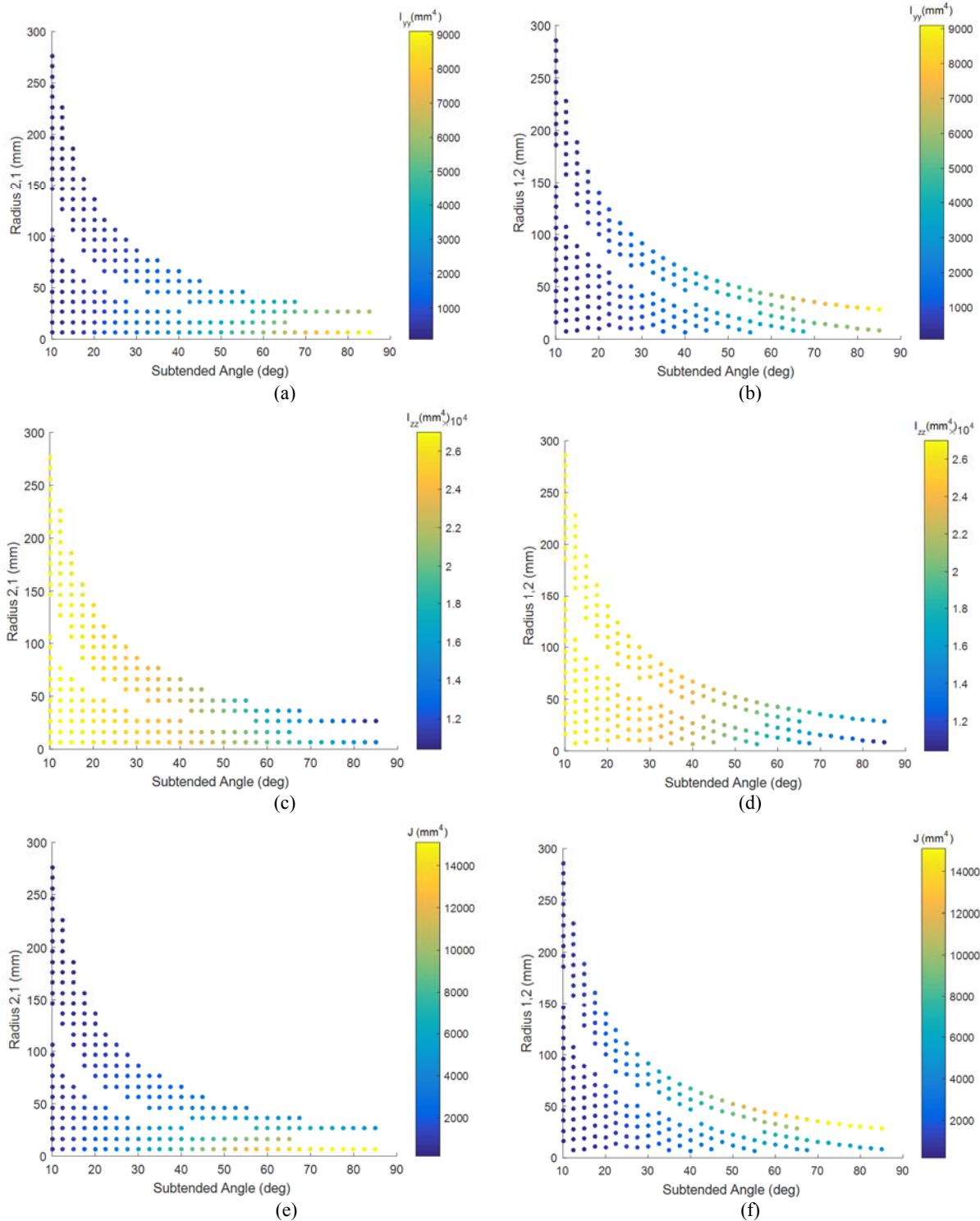
Fig. 12. Circular Bi-CTM boom parametric analysis for (a) I_{yy} vs. α vs. R_1 (or R_2), (b) I_{yy} vs. α vs. R_2 (or R_1), (c) I_{zz} vs. α vs. R_2 (or R_1), (d) I_{zz} vs. α vs. R_2 (or R_1), (e) J vs. α vs. R_2 (or R_1), and (f) J vs. α vs. R_2 (or R_1).

Higher subtended angles favor I_{yy} and J while lower values are more suited for maximizing I_{zz}. The radii of either circular segments do not affect the area moments of inertia or the torsional constant as significantly. The gaps in the parameter range signify that certain combinations of radii and subtended angles yield monostable booms and is useful as a design guide when specifying cross-sectional geometry if bistability is desired. In particular, this occurs whenever

the radii and arc lengths of segments 1 and 2 are identical and is due to the [45PW$_C$/0$_C$/45PW$_C$] outer shell having equal sections bending in the equal-sense and opposite-sense directions eliminating the second stable state. The outer shell is only bistable in equal-sense bending, and will not have an energy minimum to dwell in when bent in the opposite-sense direction. The [0-90PW$_C$] inner shell is always monostable, but will not alter the balance of the outer shell segments bending in either directions as its associated strain energies are much lower. Therefore, the ratio of segments bending in equal or opposite-sense directions is critical when attempting to induce bistability in two-shelled composite booms.

The results of the parametric study show that the area moments of inertia and torsional constant were maximized when the subtended angle is 85°, radius of segment 1 is 28.13 mm, and the radius of segment 2 is 6.25 mm for both shells. This leads to 9089 mm^4 for I_{yy}, 14257 mm^4 for I_{zz}, and 14989 mm^4 for J. Like for the bi-X boom case, the lower of the two area moments of inertia (I_{yy}) is prioritized and the resulting parameters happen to also be optimal for maximizing the torsional constant.

(a)   (b)
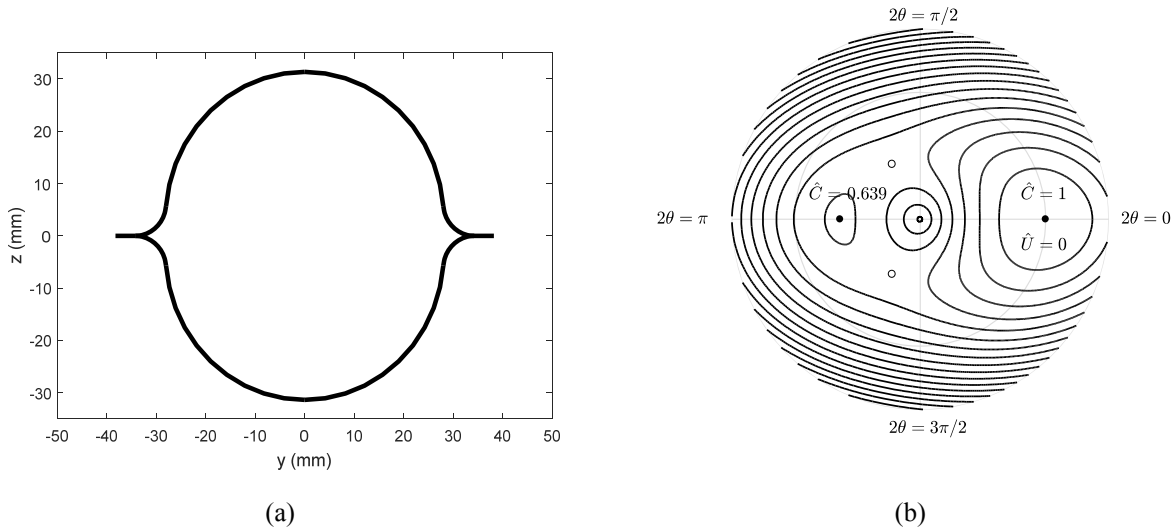
Fig. 13. (a) Optimal cross-section design of the circular Bi-CTM boom based on the parametric analysis, and corresponding (b) polar contour plot of the non-dimension strain energy per unit length, $\widehat{U}$, as a function of $\widehat{C}$ and θ. The two stable locations are marked as dots while the two unstable points are marked as circles. The contour lines are separated by a constant $\widehat{\Delta U} = 0.05$.

Fig. 13 presents the optimal cross-sectional geometry for the circular Bi-CTM boom based on the results of the parametric analysis and its corresponding non-dimensionalized strain energy per unit length polar contour plot. Like the Bi-SHEARLESS and Bi-TRAC booms in Fig. 7, the Bi-CTM boom has four equilibrium positions, with two being stable, at the extended configuration of $\hat{C} = 1$ and $\theta = 0$ and the coiled configuration of $\hat{C} = 0.639$ and $\theta = \pi/2$, which translates to a stable coiled diameter of 88.10 mm. The other two positions were unstable saddle points. Using this optimal cross-sectional geometry, a laminate study with the thin-ply materials from Table 1 was conducted using the inextensional model to determine which layups yield Bi-CTM booms. The investigated laminates and their labels for both the circular and parabolic CTMs are shown in Table 4. Note that the unidirectional carbon fiber material was different between the first half (IM MR60H) and second half (HM HS40) of the layups. Table 5 presents the model results for various circular CTM boom laminates.

Table 4. Circular and parabolic CTM boom laminate layups used in the study

Circular CTM	Parabolic CTM	Inner Shell	Outer Shell
v1	v21	[0$_C$/45PW$_{AQ}$/0$_C$]	[0$_C$/45PW$_{AQ}$/0$_C$]
v2	v22	[45PW$_{AQ}$/0$_C$/45PW$_{AQ}$]	[45PW$_{AQ}$/0$_C$/45PW$_{AQ}$]
v3	v23	[45PWc/0$_C$/45PWc]	[45PWc/0$_C$/45PWc]
v4	v24	[0-90PW$_C$]	[45PWc/0$_C$/45PWc]
v5	v25	[45PWc/0$_C$]	[45PWc/0$_C$/45PWc]
v6	v26	[45BRc/0$_C$]	[45PWc/0$_C$/45PWc]
v7	v27	[45PW$_{AQ}$/0$_C$/45PW$_{AQ}$]	[45PWc/0$_C$/45PWc]

v8	v28	$[45PW_{AQ}/0_C/45PW_{AQ}]$	$[45BRc/0_C/45BRc]$
v9	v29	$[45BRc/0_C]$	$[45PW_{AQ}/0_C/45PW_{AQ}]$
v10	v30	$[45PWc/0_C]$	$[45PWc/0_C]$
v11	v31	$[0_{CHM}/45PW_{AQ}/0_{CHM}]$	$[0_{CHM}/45PW_{AQ}/0_{CHM}]$
v12	v32	$[45PW_{AQ}/0_{CHM}/45PW_{AQ}]$	$[45PW_{AQ}/0_{CHM}/45PW_{AQ}]$
v13	v33	$[45PWc/0_{CHM}/45PWc]$	$[45PWc/0_{CHM}/45PWc]$
v14	v34	$[0-90PW_C]$	$[45PWc/0_{CHM}/45PWc]$
v15	v35	$[45PWc/0_{CHM}]$	$[45PWc/0_{CHM}/45PWc]$
v16	v36	$[45BRc/0_{CHM}]$	$[45PWc/0_{CHM}/45PWc]$
v17	v37	$[45PW_{AQ}/0_{CHM}/45PW_{AQ}]$	$[45PWc/0_{CHM}/45PWc]$
v18	v38	$[45PW_{AQ}/0_{CHM}/45PW_{AQ}]$	$[45BRc/0_{CHM}/45BRc]$
v19	v39	$[45BRc/0_{CHM}]$	$[45PW_{AQ}/0_{CHM}/45PW_{AQ}]$
v20	v40	$[45PWc/0_{CHM}]$	$[45PWc/0_{CHM}]$

According to Table 5, the circular CTM boom is bistable only if the outer shell has a 45 degree symmetric layup that also retains bistability, and the bending stiffnesses of the opposing inner shell is lower than the outer shell. The bistable outer shell bending equal-sense, must be able to overcome the inner shell's stiffness in the opposite-sense direction in order to reach the boom's second potential well. Circular CTM_v4 has the lowest stable coiled diameter and deployment load and longest allowable length, which agreed with the SHEARLESS and TRAC laminate results and further justifies the layup selection made for the parametric analysis. It should be noted that the stowed volume constraint assumed for 110-mm-tall booms was 101 mm for the outer diameter ($2\,r_f$) when a single boom was coiled ($n_b = 1$), and 210 mm for four co-reeled booms ($n_b = 4$). This was to satisfies the design requirement for the CTM booms to fit inside 12U CubeSats platforms for future solar sail exploration missions[24].

Table 5. Model results for various circular CTM boom laminate layups

Circular CTM	Bistability Criterion Value	Model Bi-stable	Stable Model Diameter (mm)	Length Allowed - 1 Boom /4 Co-reeled Booms (m)	Bistability Limit Length - 1 Boom (m)	Deployment Force (N)	I_{yy} (mm^4)	I_{zz} (mm^4)	J (mm^4)
v1	0.00000	No	N/A	N/A	N/A	N/A	11794	15918	20959
v2	0.00000	No	N/A	N/A	N/A	N/A	13258	17783	23560
v3	0.00000	No	N/A	N/A	N/A	N/A	15136	20176	26898
v4	0.00960	Yes	88.10	4.87 / 18.13	11.06	0.50	9090	14257	14989
v5	0.00370	Yes	110.34	Exceeds Limit/14.30	7.02	0.62	11734	16451	20460
v6	0.00240	Yes	117.38	Exceeds Limit/13.43	5.16	0.66	11995	16698	20979
v7	0.00057	Yes	125.17	Exceeds Limit/11.39	1.30	0.82	14154	18980	25118
v8	-0.00053	No	N/A	N/A	N/A	N/A	14501	19472	25702
v9	-0.00064	No	N/A	N/A	N/A	N/A	11276	15501	19881
v10	0.00000	No	N/A	N/A	N/A	N/A	9290	12727	16508
v11	0.00000	No	N/A	N/A	N/A	N/A	9713	13266	17261
v12	0.00000	No	N/A	N/A	N/A	N/A	12217	16457	21711
v13	0.00000	No	N/A	N/A	N/A	N/A	14095	18851	25049
v14	0.00720	Yes	89.01	4.71 / 18.70	10.75	0.43	8810	13594	14687
v15	0.00330	Yes	108.84	Exceeds Limit/15.40	8.04	0.50	10650	15125	18495
v16	0.00210	Yes	116.76	Exceeds Limit/14.37	5.82	0.54	10918	15372	19033
v17	0.00092	Yes	121.27	Exceeds Limit/12.47	2.54	0.65	13110	17654	23261
v18	0.00002	Yes	126.77	Exceeds Limit/11.63	0.05	0.77	13454	18147	23837
v19	-0.00046	No	N/A	N/A	N/A	N/A	10217	14175	17982
v20	0.00000	No	N/A	N/A	N/A	N/A	8249	11401	14660

C. Parabolic Bi-CTM Boom

The parabolic Bi-CTM boom was investigated along with the circular version to determine if the former provides any stiffness advantages over the latter. The two independent parameters that were freely varied are the segment 1 parabola's y-range and arc length, which determine the parabola function with Eq. 14 and Eq. 15. The parabola was then discretized into circular arcs using the biarc interpolation with an allowable error of 0.01 mm. By varying the arc length and y-range, the parabola height, circular segment 2's arc length, radius, and subtended angles were all set and cannot be specified since the flattened height and web width were constant. This was to ensure tangent continuity between the last parabola biarc and the circular segment. The parabola arc length was varied from 20 mm to 102 mm in 2 mm intervals, the y-range was varied from ±10 mm to ±$\frac{L_p}{2}$, half the parabola arc length, in 1 mm intervals that correspond to the parabola height of 4 to 35 mm. The upper arc length limit of 102 mm was established from the flattened height and web width values. All combination of parameters that yield a radius of less than 6.25 mm in any parabola biarcs or the circular arc were not sampled. Since the closed-form criterion for the parabolic Bi-CTM was not derived, $\frac{\partial^2 \hat{U}}{\partial \theta^2}$ was numerically found on a case by case basis to determine bistability during the parametric analysis. Figure 14 shows how the parabolic Bi-CTM area moments of inertia and torsional constant vary with the parabola height and length. Note that the parabola height is presented as the main parameter instead of its y-range since this is easier to visualize.
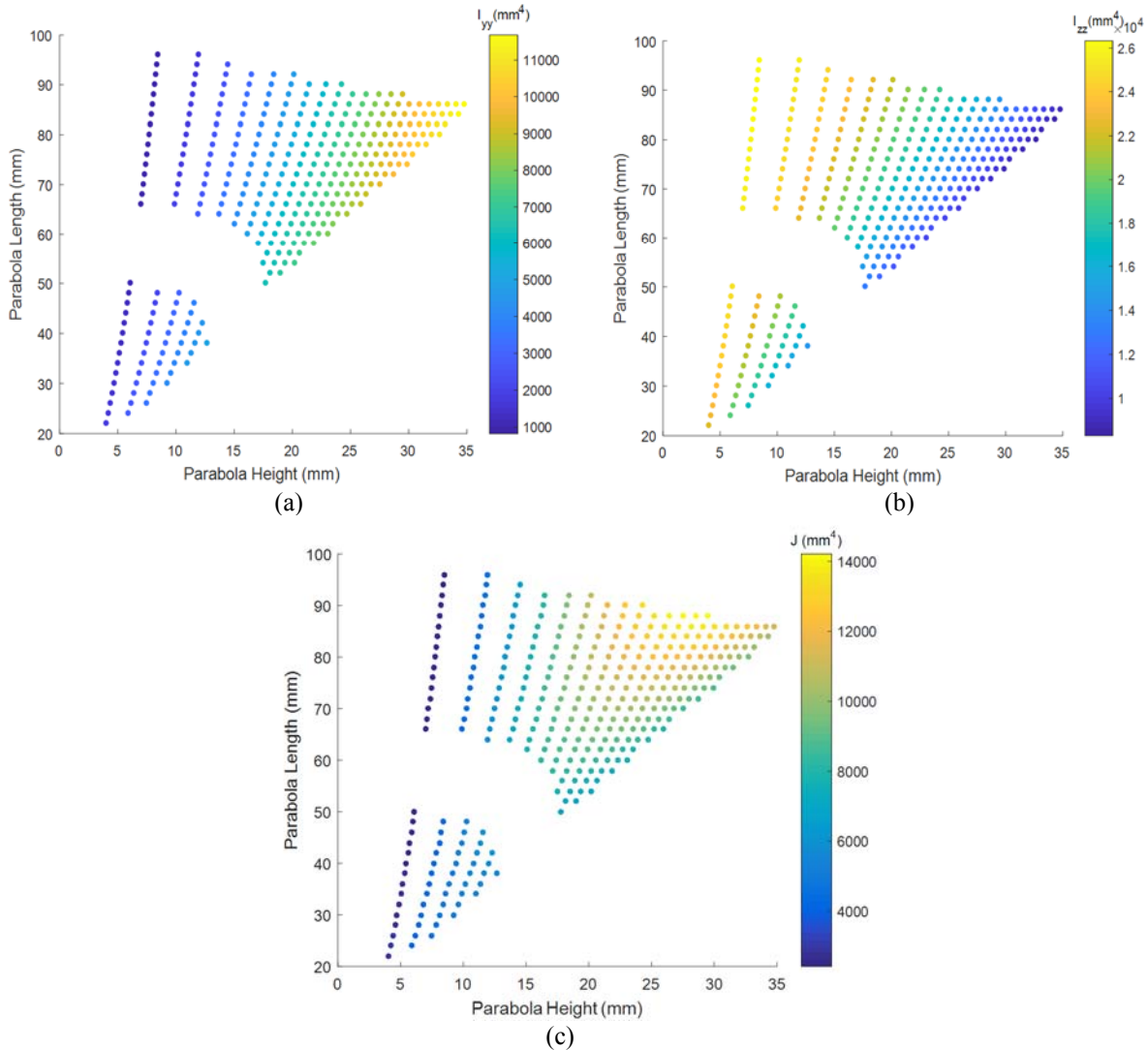

(a)

(b)

(c)

Fig. 14. Parabolic Bi-CTM boom parametric analysis against parabola height and length for (a) I_{yy}, (b) I_{zz}, and (c) J.

According to Fig. 14, I_{yy} was consistently favored by higher parabola heights across all parabolic arc lengths, and lower heights favor I_{zz}. In contrast, the upper ranges of parabola arc length and height maximized the torsional constant. As in Fig. 12, the gaps in the sampled points signify that combinations of parabola heights and arc lengths which yield a segment 1 that was similar to the circular segment 2 results in a monostable boom, for the same reasons that the gap appears for the circular Bi-CTM parametric analysis.

The optimal cross-section where the two area moments of inertia intersect was when the parabola height and arc length were 32.6 mm and 86 mm. The circular arc length of segment 2 is 6.64 mm and its subtended angle is 69°. This resulted in 10685 mm⁴ for I_{yy}, 10814 mm⁴ for I_{zz}, and 12514 mm⁴ for J. Getting consistent area moments of inertia were prioritized over maximizing the torsional constant, but the resulting optimal cross-section yields a J value that was fairly close to the upper limit in the parametric study. The optimal parabolic Bi-CTM had higher I_{yy} and lower I_{zz} and J values when compared to its circular counterpart, and shows more consistent bending stiffnesses between the y and z directions. If the objective is to have uniform performance in withstanding lateral loads at the expense of a lower torsional stiffness, then the parabolic Bi-CTM is the preferred configuration.

(a)   (b)
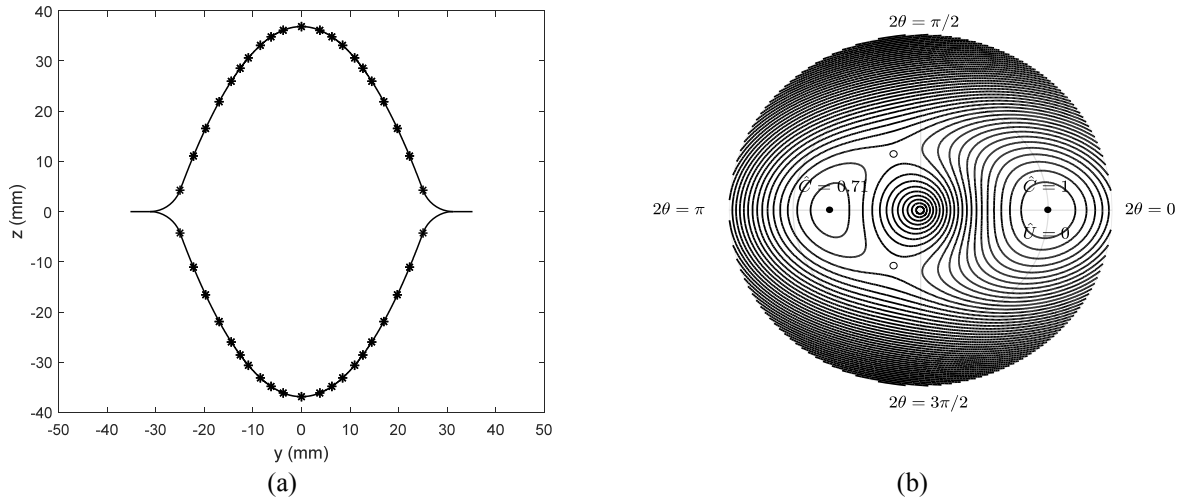
Fig. 15. (a) Optimal cross-section of the parabolic Bi-CTM based on the parametric analysis with asterisks indicating biarc discretization, and corresponding (b) polar contour plot of $\widehat{U}$ as a function of $\widehat{C}$ and θ. The two stable locations are marked as dots while the two unstable points are marked as circles. The contour lines are separated by a constant $\widehat{\Delta U} = 0.05$.

Figure 15 presents the optimal cross-sectional geometry for the parabolic Bi-CTM boom based on the results of the parametric analysis, and its corresponding non-dimensionalized strain energy per unit length polar contour plot. The asterisks in the cross-section indicate where the parabola was discretized into circular arcs. It has two stable equilibrium points, at the extended state of $\hat{C} = 1$ and $\theta = 0$ and the coiled state of $\hat{C} = 0.710$ and $\theta = \pi/2$, which translates to a stable coiled diameter of 75.40 mm. Although its coiled diameter was lower than the circular Bi-CTM of the same flattened height and web width, the associated strain energy in the contour plot was much higher. Table 6 presents the model results for various parabolic CTM boom laminates, where the layup details are shown in Table 4.

Table 6. Model results for various parabolic CTM boom laminates

Parabolic CTM	Model Bi-stable	Stable Model Diameter (mm)	Length Allowed - 1 Boom / 4 Co-reeled Booms (m)	Bistability Limit Length - 1 Boom (m)	Deployment Force (N)	I_{yy} (mm⁴)	I_{zz} (mm⁴)	J (mm⁴)
v21	No	N/A	N/A	N/A	N/A	13776	12065	17498
v22	No	N/A	N/A	N/A	N/A	15486	13470	19670
v23	No	N/A	N/A	N/A	N/A	17680	15272	22457
v24	Yes	75.40	9.02 / 19.17	9.78	7.44	10685	10814	12514
v25	Yes	94.45	2.30 / 15.76	6.65	9.81	13729	12467	17082
v26	Yes	100.48	0.18 / 15.06	5.23	10.46	14031	12652	17515
v27	Yes	107.14	Exceeds Limit / 13.07	2.17	13.23	16535	14371	20971
v28	Yes	112.06	Exceeds Limit / 12.38	0.26	15.64	16942	14742	21458

v29	No	N/A	N/A	N/A	N/A	13180	11751	16598
v30	No	N/A	N/A	N/A	N/A	10851	9662	13783
v31	No	N/A	N/A	N/A	N/A	11345	10068	14411
v32	No	N/A	N/A	N/A	N/A	14271	12471	18127
v33	No	N/A	N/A	N/A	N/A	16464	14274	20913
v34	Yes	76.15	9.10 / 19.80	9.59	6.39	10346	10315	12262
v35	Yes	93.13	2.92 / 16.91	7.52	7.91	12465	11468	15441
v36	Yes	99.92	0.41 / 16.09	5.83	8.52	12774	11654	15890
v37	Yes	103.77	Exceeds Limit / 14.14	3.18	10.49	15316	13372	19420
v38	Yes	108.49	Exceeds Limit / 13.42	1.26	12.53	15719	13743	19901
v39	No	N/A	N/A	N/A	N/A	11944	10753	15013
v40	No	N/A	N/A	N/A	N/A	9636	8664	12239

The results in Table 6 follow the trend of the circular CTM booms in Table 5, where the outer shell must have a bistable layup and the inner shell must be the more compliant laminate. The only difference was that the parabolic CTM_v28 was bistable when the circular CTM_v8 with the identical layup, and material was not. This, in combination with the lower stable coiled diameters and the longer allowable lengths, indicate that it was easier to induce bistability in the optimal parabolic CTM boom when compared to the circular counterpart.

Both the optimal circular v4 and parabolic v24 CTM booms were recently manufactured, but they turned out to be monostable revealing that the simple inextensional model was not able to predict bistability for the optimal CTM boom shape investigated in this section. A more in-depth experimental and analytical study on these booms with varying materials, asymmetrical layups and geometries for each shell, and designs specifically catered towards generating bistability will be conducted in future work.

VIII. Conclusion

This paper presented an inextensional analytical model that predicts the stable configurations of two-shelled bistable composite booms, which can remain in an extended and a coiled state without any energy input. A variety of different boom types using two cylindrical laminate shells that were bonded or held together were investigated, including the SHEARLESS, TRAC, X, circular CTM, and parabolic CTM booms. These structures are deployable composite boom candidates for upcoming NASA solar sail technology demonstration missions[24] and future small satellite applications with CubeSats as one of the platforms[14].

The two-parameter model was adjusted for each boom type so that the bending strain energies of each shell or their segments are found separately, and then combined in the energy minimization formulations. Bistability criteria were then derived for each boom type by evaluating the stability of the second equilibrium state in order to determine which design parameters were critical for inducing bistability. The various criteria found allow the direct evaluation of bistability without the need for minimizing the strain energy, which was particularly useful during parametric studies. It appears that bistability in Bi-SHEARLESS booms depends on the laminate stiffness parameters of its shells and not on cross-section geometry, as opposed to the rest of the boom types. The Bi-CTM boom concepts studied have the strongest dependency on geometry for achieving bistability, as they depend, aside from the flattened height and web width as in the case of Bi-TRAC and Bi-X booms, on the arc lengths and radii of every segment. Bending stiffnesses of both the inner and outer shells have the most influence on whether a second strain energy minimum can be generated for all boom types, and cross-sectional geometric parameters also affect the TRAC, X, and CTM booms.

The predicted stable coiled diameters were compared with past experimental data for the SHEARLESS and TRAC booms as preliminary validation for the model. For these cases, the model was able to distinguish between monostable and bistable booms with fairly good agreement in the coiled diameter. Parametric design studies were then conducted to determine the optimal cross-sectional geometries for each boom type that maximize their area moments of inertia and torsional constant while meeting mission requirements and retaining bistability.

For the optimal CTM boom design, the current model incorrectly predicts bistability, and so future work will explore its full merit by designing and fabricating bistable CTM half shells and booms of varying materials, laminates, and geometries. In addition, the design space of two-shelled bistable composite booms will be expanded with more experimental data from fabricated specimens and finite element analysis for complete validation of the derived model.

Acknowledgments

References

[1]Mar, J., Garrett, T., "Mechanical Design and Dynamics of the Alouette Spacecraft." *Proceedings of the IEEE*, Vol. 57, No. 6, 1969, pp. 882-896.

[2]Kebadze, E., Guest, S. D., Pellegrino, S., "Bistable Prestressed Shell Structures." *International Journal of Solids and Structures*, Vol. 4, 2004, pp. 2801-2820.

[3]Iqbal, K., Pellegrino, S. "Bistable Composite Shells*." 41st AIAA Structures, Structural Dynamics, and Materials Conference*. Atlanta, GA, 3-6 April 2000.

[4]Fernandez, J. M., et al., "Design and Development of a Gossamer Sail System for Deorbiting in Low Earth Orbit", *Acta Astronautica*, Vol. 103, 2014, pp. 204-225.

[5]Ayre, M., "Biomimetics Applied to Space Exploration", in *Design and Nature II*, edited by Collins, M.W., Brebbia, C. A.

[6]Daton-Lovett, A. J., "An Extendible Member", U.S. Patent 6217975 B1, filed on 25 Mar. 1996 and published on 17 Apr. 2001.

[7]Iqbal, K., Pellegrino, S., Daton-Lovett, A. J., "Bistable Composite Slit Tubes*." IUTAM-IASS Symposium on Deployable Structures*. Cambridge, UK, 6-9 September 1998.

[8]Murphey, T. W., Pellegrino, S. "A Novel Actuated Composite Tape-Spring for Deployable Structures*." 45th AIAA Structures, Structural Dynamics, and Materials Conference*. Palm Springs, CA, USA, 19-22 April 2004.

[9]Schultz, M., Hulse, M., Keller, P., Turse, D., "Neutrally Stable Behavior in Fiber-Reinforced Composite Tape Springs." *Composites, Part A*, Vol. 39, 2008, pp. 1012-1017.

[10]Fernandez, J. M., Viquerat, A., Lappas, V. J. Daton-Lovett, A. J., "Bistable Over the Whole Length (BOWL) CFRP Booms for Solar Sails", *Advances in Solar Sailing*, edited by MacDonald, M., Springer Praxis Books, Springer-Verlag Berlin Heidelberg, 2014, pp. 609-628.

[11]Galletly, D. A., Guest, S. D., "Bistable Composite Slit Tubes. I. A Beam Model", *International Journal of Solids and Structures*, Vol. 41, No. 16, 2004, pp. 4517-4533.

[12]Galletly, D. A., Guest, S. D., "Bistable Composite Slit Tubes. II. A Shell Model", *International Journal of Solids and Structures*, Vol. 41, No. 16, 2004, pp. 4503-4516.

[13]Guest, S., D., Pellegrino, S., "Analytical Models for Bistable Cylindrical Shells". *Proceedings of the Royal Society A*, Vol. 462, 2006, pp. 839-854.

[14]Fernandez, J. M. "Advanced Deployable Shell-Based Composite Booms for Small Satellite Applications including Solar Sails*", 4th International Symposium on Solar Sailing*, Kyoto, Japan, 17-20 Jan. 2017.

[15]Fernandez, J. M., "Sheath-Based Rollable Lenticular-Shaped and Low-Stiction Composite Boom", U.S. Patent 20170058524 A1, filed on 24 August 2016 and published on 2 March 2017.

[16]Fernandez, J. M., et al., "Deployment Mechanisms of a Gossamer Satellite Deorbiter", *15th European Space Mechanisms & Tribology Symposium*, Noordwijk, The Netherlands, 25-27 Sept. 2013.

[17]Fernandez, J. M., "Low-Cost Gossamer Systems for Solar Sailing and Spacecraft Deorbiting Applications", PhD Dissertation, Surrey Space Center, University of Surrey, Guildford, UK, 2014.

[18]Murphey, T. W., Banik, J., "Triangular Rollable And Collapsible Boom", U.S. Patent 7895795 B1, filed on 22 October 2007 and published on 1 March 2011.

[19]Murphey, T. W., Turse, D. E., Adams, L. G. "TRAC Boom Structural Mechanics", *4th AIAA Spacecraft Structures Conference, AIAA SciTech 2017 Forum,* Grapevine, TX, 9-13 Jan. 2017.

[20]Leclerc, C., Wilson, L., Bessa, M.A., Pellegrino, S., "Characterization of Ultra-Thin Composite Triangular Rollable And Collapsible Booms", *4th AIAA Spacecraft Structures Conference, AIAA SciTech 2017 Forum,* Grapevine, TX, 9-13 Jan. 2017.

[21]Abrams, J. L., Rakow, A., Duchek, M., Harbach, R., "X-Boom", NASA SBIR Phase I Final Report, Analytical Mechanics Associates, Inc., Denver, CO, 16 December 2015. SBIR contract number NNX15CL81P.

[22]Abrams, J. L., Ducheck, M. E., Paz, A., Harbach, R. A., "Extendable Solar Array", U.S. Patent 20160122041 A1, filed on 8 October 2015 and published on 5 May 2016.

[23]Fernandez, J. M., et al., "NASA's Advanced Solar Sail Propulsion System for Low-Cost Deep Space Exploration and Science Missions that Use High Performance Rollable Composite Booms", *4th International Symposium on Solar Sailing*, Kyoto, Japan, 17-20 Jan. 2017.

[24]Fernandez, J. M., et al., "An Advanced Composites-Based Solar Sail System for Interplanetary Small Satellite Missions", *5th AIAA Spacecraft Structures Conference, AIAA Scitech 2018 Forum*, Kissimmee, FL, 8-12 Jan. 2018.

[25]Bolton, K. M., Biarc curves, *Computer Aided-Design*, Vol. 7, 1975, pp. 98-92.

[26]Meek, D. S., Walton, D. J., "Approximating Smooth Planar Curves by Arc Splines", *Journal of Computational and Applied Mathematics*, Vol. 59, 1995, pp. 221-231.

[27]Yang, X., "Efficient Circular Arc Interpolation based on Active Tolerance Control", *Computer-Aided Design*, Vol. 34, 2002, pp. 1037-1046.

[28]Jeon, S. K., Murphey, T. W., "Design and Analysis of a Meter-Class CubeSat Boom with a Motor-less Deployment by Bi-stable Tape Springs", *52nd AIAA Structures Structural Dynamics and Materials Conference*. Denver, CO, USA, 4-7 April 2011.

[29]NASA Space Technology Mission Directorate, Game Changing Development Program, URL: http://gameon.nasa.gov/projects/deployable-composite-booms-dcb